Model verification, updating, and selection from the constitutive relation error concept

Ludovic Chamoin, P. Ladevèze

Model verification, updating, and selection from the Constitutive Relation Error concept

L. Chamoin[a,b,*], P. Ladevèze[a]

[a] *Universite Paris-Saclay, CentraleSupelec, ENS Paris-Saclay, CNRS, LMPS - Laboratoire de Mecanique Paris-Saclay, 4 avenue des Sciences, Gif-sur-Yvette, 91190, France*
[b] *Institut Universitaire de France, 1 rue Descartes, Paris, 75231, France*

Abstract

This chapter is a review on the energy-based Constitutive Relation Error (CRE) concept which has been developed for more than 40 years as a general verification tool in finite element simulations. It turns out that this concept is suitable to a posteriori compute some strict and effective bounds on the discretization error for a large set of structural mechanics problems. We show here the basic features of CRE-based error estimation, as well as more recent developments dealing with goal-oriented error estimation or the control of reduced order models. In addition, we also show how the CRE concept can be beneficially used together with experimental information, in order to conduct inverse analysis with model updating, as well as to question the relevance of the employed mathematical model by using model selection, enrichment, or learning. Illustrative examples are shown for these various applications of the CRE concept.

Keywords: Constitutive Relation Error, A posteriori error estimation, Goal-oriented strategy, Model reduction, Parameter identification, Constitutive modeling

*corresponding author

Email addresses: ludovic.chamoin@ens-paris-saclay.fr (L. Chamoin), pierre.ladeveze@ens-paris-saclay.fr (P. Ladevèze)

1. Introduction

Modeling and simulation have nowadays become a central engineering activity, both in industry and in research. In this activity, a constant concern has always been the mastering of mathematical and numerical models which may attain high complexity levels [131]. Over the last 40 years, quantitative tools have appeared in order to assess the quality of simulation results, especially when derived from Finite Element (FE) analysis, with respect to a reference mathematical model [2, 105, 33]; this topic is now known as model verification and is extensively developed in computational mechanics. While only estimates on the global discretization error were available until the 1990's, with associated local error indicators and adaptive strategies, goal-oriented error estimation techniques have emerged since then in order to address the key issue of evaluating the quality of local quantities of interest resulting from a FE simulation and useful for design purposes. The main idea in this achievement is that a quantity of interest can be written globally, thus allowing the reuse of global error estimators [12, 142, 147]. However, accurate error estimation requires the approximate solution of an adjoint problem [77].

In this broad context of FE model verification, we focus here on a general approach referring to the Constitutive Relation Error (CRE) concept. It provides for guaranteed, accurate, and fully computable error bounds, which is a main advantage for robust design. It is based on a simple and consistent idea: all exact equations of the mathematical problem defined over the space-time domain (e.g., equilibrium and compatibility equations) should be satisfied by so-called admissible fields except the constitutive relation which is less reliable as empirically chosen and depending on experimental data; the residual on the satisfaction of this constitutive relation thus constitutes an (energy-based) error indicator for the approximate solution. Of course, the construction of such admissible fields and in particular a fully equilibrated dual field is a technical point in the approach [93, 97, 72, 123, 60, 111, 143]. Developed in the late 1970s for a posteriori error estimation on linear problems solved with FEM [92, 93, 53], the CRE concept has been extended and applied to nonlinear time-dependent problems in structural mechanics over the years (an overview can be found in [105, 115]) to perform global error estimation and lead adaptive procedures. These include (visco-)plasticity and damage [70, 99, 102, 103, 141, 104], addressed through the standard thermodynamics framework of stable materials with internal variables [81, 74],

contact-friction problems [44, 117, 164], as well as dynamics [94, 43]. In this framework, convexity and duality properties are a key point to recover mathematical properties for error bounds. Also, the CRE approach unifies a set of powerful verification methods around the concept of equilibrium which is actually the only way to recover mathematically guaranteed and fully computable error bounds; let us mention in this category the (implicit) element residual method with equilibration [9, 1], smoothing techniques with equilibrium constraints [163, 20, 150], or the subdomain residual method with flux-free technique [138, 45, 139].
During the last two decades, the CRE concept was extensively used to get strict and accurate error bounds on outputs of interest, both for linear and time-dependent nonlinear problems (e.g., see [107, 23, 24, 109, 110, 25, 113, 158, 114, 160, 161]). These works associated with key technical points often lead to first bounds of this kind in the literature, taking all error sources (time and space discretizations, iteration stopping) into account. Out of standard FEM, the CRE concept was also applied to more advanced discretization techniques such as XFEM [71, 135, 136], isogeometric analysis (IGA) [156, 30], non-conforming FEM [52, 61], domain decomposition techniques [140, 149], stochastic approaches [108, 25], or MsFEM in multiscale approaches [29, 31], as well as to PGD model reduction [112, 28, 30, 148]. Also, the CRE concept was recently implemented for model verification in the context of deep learning, controlling generalization errors in approximations of elasticity problems obtained from a mixed form of Physics-Informed Neural Networks (PINNs) [80].
Basic concepts of CRE and several of the CRE-based tools developed for a posteriori model verification are reviewed in a first part of the chapter.

Another critical aspect to certify the quality of numerical simulations outputs is to question the quality of the mathematical model itself, that is its capability to represent a faithful abstraction of the physical system being studied. This integrates the identification or updating of model parameters from experimental measurements, leading to the solution of an inverse problem. In this context where the material behavior is a major component, the CRE concept again appears as a sound, convenient, and powerful tool. First developments were made in the 1990s for dynamics models [96, 41, 42, 100], before being successfully used in many applications of inverse problems such as forced vibrations [50, 11, 51, 8, 54, 153, 79, 55, 151, 57, 152], transient dynamics [5, 65, 128, 19], acoustics [48, 49, 162, 146], probabilistic

models (when considering a family of similar structures) [106, 64], joint or connexion identification problems [73, 132, 133], nonlinear material behaviors [128, 78, 120, 129], in-situ measurements [35, 21], or full-field measurements from imaging [134, 14, 86, 76, 66, 129]. After first works in which measurements were included as additional admissibility constraints, a more flexible and effective strategy denoted as modified CRE (mCRE) was developed. It consists in a hybrid variational formulation where constraints on measurements and other uncertain data are released. It thus proposes a general framework driven by reliability of information: reliable theoretical and experimental information (equilibrium, sensor position, etc.) is favored to define admissibility spaces and is strongly enforced in the inversion process, while complementary information (material behavior, sensor measurement values, etc.) is released and satisfied at best. A residual associated with this complementary information is then measured. The minimization of the mCRE cost function, which is a nonlinear contraint optimization problem, is then performed by means of an iterative two-steps algorithm where optimal admissible fields are first computed, before minimizing with respect to model parameters.

It was shown that the mCRE functional provides for an appropriate metric in inverse problems, mixing a metric on discrepancy with measurements and a metric on the modeling space. Its use presents interesting advantages for identification purposes compared to some alternative techniques; out of improved convexity properties (over its least-squares counterpart) and tolerance to incompletely specified boundary conditions [18, 65, 54, 7], it has excellent capacities to localize structural defects spatially [22, 63, 8, 14, 19, 10, 85, 58], and it is very robust to noisy or corrupted measurements [5, 65, 128, 14]. Also, the system state estimated from mCRE (in terms of optimal admissible fields) can be interpreted as an hybrid twin as defined in [39], with a compromise between physics-based and data-based modeling, and taking the best of both worlds by accounting for modeling bias while correcting it from data (data-based enrichment of the a priori chosen mathematical model). Moreover, the CRE term of the mCRE functional can be seen as a quantitative modeling error indicator, which may be beneficially used for optimal physics-constrained model definition from data. This may be performed by selecting the appropriate model in a list of model classes (e.g. constitutive law structures) [130], or by using deep learning techniques to determine model ignorance [15, 16, 116]. Recently, the mCRE approach was also extended to sequential data assimilation by inserting it into a Kalman

filtering strategy [119, 56]. In the context of Structural Health Monitoring (SHM) [62], this new methodology constitutes a powerful tool to perform online SHM [34] and more generally address Dynamic Data Driven Applications Systems (DDDAS) challenges as defined in [46] in which data are seamlessly integrated with digital twins.
The overall use of the CRE concept together with experimental data is developed in the second part of the chapter, with typical applications tackled in recent works.

2. Model verification with the CRE concept

In this section, we first give the main features of the CRE approach, based on duality analysis, for a posteriori error estimation in FEM simulation. We go into further details for the elasticity case alone, even though extensions to nonlinear time-dependent problems are also given. Then, we present more recent works on the use of the CRE error estimate to control the quality of reduced order modeling.

2.1. Reference elasticity problem and FEM approximation

We consider an open bounded domain $\Omega \subset \mathbb{R}^d$ ($d = 1, 2, 3$) with Lipschitz boundary $\partial\Omega$, occupied by an elastic material (Fig. 1). We assume that a displacement field $\mathbf{u}_d \in [H^{1/2}(\partial_1\Omega)]^d$ is prescribed on $\partial_1\Omega \subset \partial\Omega$ (Dirichlet boundary condition) with $\partial_1\Omega \neq \emptyset$, and that tractions $\mathbf{F}_d \in [H^{-1/2}(\partial_2\Omega)]^d$ are prescribed on the complementary part $\partial_2\Omega$ (Neumann boundary condition) such that $\partial_1\Omega \cap \partial_2\Omega = \emptyset$ and $\overline{\partial_1\Omega \cup \partial_2\Omega} = \partial\Omega$. A body force field $\mathbf{f}_d \in [L^2(\Omega)]^d$ may also be given in Ω. We assume small displacements, quasi-static loading, and isothermal conditions.
The associated (well-posed) problem consists in finding the solution pair $(\mathbf{u}, \boldsymbol{\sigma})$ which satisfies:

- kinematic equations:

$$\mathbf{u} \in [H^1(\Omega)]^d \quad ; \quad \mathbf{u}_{|\partial_1\Omega} = \mathbf{u}_d \tag{1}$$

- equilibrium equations:

$$\boldsymbol{\sigma} \in [L^2(\Omega)]^{d(d+1)/2}_{sym} \quad ; \quad \nabla \cdot \boldsymbol{\sigma} + \mathbf{f}_d = \mathbf{0} \text{ in } \Omega \quad ; \quad \boldsymbol{\sigma}\mathbf{n}_{|\partial_2\Omega} = \mathbf{F}_d \tag{2}$$

- constitutive relation:

$$\boldsymbol{\sigma} = \boldsymbol{C}\left(\boldsymbol{\epsilon}(\mathbf{u})\right) \tag{3}$$

$\boldsymbol{\epsilon}(\mathbf{u}) \equiv \frac{1}{2}(\nabla \mathbf{u} + \nabla^T \mathbf{u})$ denotes the linearized strain tensor, $\boldsymbol{\sigma}$ is the Cauchy stress tensor, and $\boldsymbol{C}$ is the elasticity tensor.

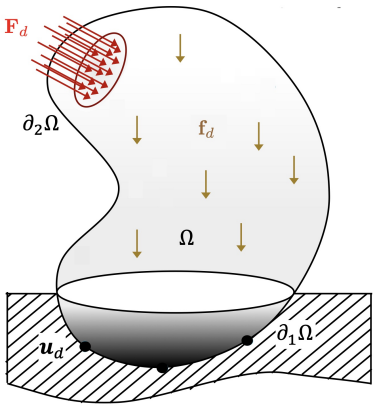

Figure 1: Configuration of the reference problem.

We introduce the following admissibility spaces:

- the space $\boldsymbol{\mathcal{U}}_{ad}$ of kinematically admissible displacement fields:

$$\boldsymbol{\mathcal{U}}_{ad} \equiv \left\{ \mathbf{v} \in [H^1(\Omega)]^d | \ \mathbf{v} \text{ satisfies } (1) \right\} \tag{4}$$

- the space $\boldsymbol{\mathcal{S}}_{ad}$ of statically admissible stress fields:

$$\boldsymbol{\mathcal{S}}_{ad} \equiv \left\{ \boldsymbol{\tau} \in [H(div, \Omega)]^d | \ \boldsymbol{\tau} \text{ satisfies } (2) \right\} \tag{5}$$

Introducing the vectorial space $\boldsymbol{\mathcal{U}}_{ad,0}$ associated with $\boldsymbol{\mathcal{U}}_{ad}$, equilibrium equations can be rewritten in the following weak form of the principle of virtual work:

$$-\int_\Omega \boldsymbol{\sigma} : \boldsymbol{\epsilon}(\mathbf{v}) \mathrm{d}\Omega + \int_\Omega \mathbf{f} \cdot \mathbf{v} \mathrm{d}\Omega + \int_{\partial_2\Omega} \mathbf{F} \cdot \mathbf{v} \mathrm{d}S = 0 \quad \forall \mathbf{v} \in \boldsymbol{\mathcal{U}}_{ad,0} \tag{6}$$

Based on the thermodynamics framework with standard formulation introduced in [81] for stable materials, the constitutive relation may be expressed by means of a free energy (positive and convex) potential ψ, or its dual ψ^*, as:

$$\boldsymbol{\sigma} = \frac{\partial \psi}{\partial \boldsymbol{\epsilon}} \quad \text{or} \quad \boldsymbol{\epsilon} = \frac{\partial \psi^*}{\partial \boldsymbol{\sigma}} \tag{7}$$

Duality is here defined by the work bilinear form, by means of the Legendre-Fenchel transform [125]:

$$\psi^*(\boldsymbol{\sigma}) \equiv \sup_{\boldsymbol{\epsilon}} \left[\boldsymbol{\sigma} : \boldsymbol{\epsilon} - \psi(\boldsymbol{\epsilon})\right] \tag{8}$$

Remark 1. *In the linear elasticity case, the constitutive relation reads:*

$$\boldsymbol{\sigma} = \mathbf{K}\boldsymbol{\epsilon}(\mathbf{u}) \tag{9}$$

where $\mathbf{K}$ *is the symmetric positive definite Hooke tensor. The associated thermodynamic potentials are then quadratic and read:*

$$\psi(\boldsymbol{\epsilon}) = \frac{1}{2}\boldsymbol{\epsilon} : \mathbf{K}\boldsymbol{\epsilon} \quad ; \quad \psi^*(\boldsymbol{\sigma}) = \frac{1}{2}\boldsymbol{\sigma} : \mathbf{K}^{-1}\boldsymbol{\sigma} \tag{10}$$

Using a conforming FE method, and approximation $\mathbf{u}_h \in \boldsymbol{\mathcal{U}}_{ad}$ of $\mathbf{u}$ is computed with associated approximate stress field $\boldsymbol{\sigma}_h \notin \boldsymbol{\mathcal{S}}_{ad}$. This leads to the discretization error field $\mathbf{e}_h = \mathbf{u}_h - \mathbf{u}$, and the objective of model verification is to compute an a posteriori estimate on this error measured in some given norm (to start, in the global energy norm).

2.2. CRE definition and a posteriori estimation on discretization error

The CRE measure refers to the previously introduced Legendre-Fenchel duality, and is related to the symmetrized Bregman divergence used in statistics. For any displacement field $\hat{\mathbf{u}} \in \boldsymbol{\mathcal{U}}_{ad}$ and any equilibrated stress field $\hat{\boldsymbol{\sigma}} \in \boldsymbol{\mathcal{S}}_{ad}$, we define the CRE functional $\mathcal{E}_{CRE}$ as:

$$\mathcal{E}_{CRE} : \boldsymbol{\mathcal{U}}_{ad} \times \boldsymbol{\mathcal{S}}_{ad} \mapsto \mathbb{R} \; ; \quad \mathcal{E}^2_{CRE}(\hat{\mathbf{u}}, \hat{\boldsymbol{\sigma}}) \equiv \int_\Omega \left[\psi(\boldsymbol{\epsilon}(\hat{\mathbf{u}})) + \psi^*(\hat{\boldsymbol{\sigma}}) - \hat{\boldsymbol{\sigma}} : \boldsymbol{\epsilon}(\hat{\mathbf{u}})\right] \mathrm{d}\Omega \geq 0 \tag{11}$$

It corresponds to a measure of the residual on the constitutive relation for the admissible pair $(\hat{\mathbf{u}}, \hat{\boldsymbol{\sigma}}) \in \boldsymbol{\mathcal{U}}_{ad} \times \boldsymbol{\mathcal{S}}_{ad}$, and it naturally yields the following property:

$$\begin{aligned} \mathcal{E}^2_{CRE}(\hat{\mathbf{u}}, \hat{\boldsymbol{\sigma}}) = 0 \quad &\Longleftrightarrow \quad (\hat{\mathbf{u}}, \hat{\boldsymbol{\sigma}}) \text{ satisfies the constitutive relation (3) over } \Omega \\ &\Longleftrightarrow \quad (\hat{\mathbf{u}}, \hat{\boldsymbol{\sigma}}) \text{ corresponds to the exact solution } (\mathbf{u}, \boldsymbol{\sigma}) \end{aligned} \tag{12}$$

Remark 2. *In the linear elasticity case, the CRE functional reads:*

$$\mathcal{E}^2_{CRE}(\hat{\mathbf{u}}, \hat{\boldsymbol{\sigma}}) = \frac{1}{2}\int_\Omega (\hat{\boldsymbol{\sigma}} - \mathbf{K}\boldsymbol{\epsilon}(\hat{\mathbf{u}})) : \mathbf{K}^{-1}(\hat{\boldsymbol{\sigma}} - \mathbf{K}\boldsymbol{\epsilon}(\hat{\mathbf{u}}))\, d\Omega \tag{13}$$

A geometrical interpretation of the CRE measure is given in Fig. 2: for a given point $(\hat{\mathbf{u}}, \hat{\boldsymbol{\sigma}}) \in \boldsymbol{\mathcal{U}}_{ad} \times \boldsymbol{\mathcal{S}}_{ad}$, the value $\psi(\boldsymbol{\epsilon}(\hat{\mathbf{u}}))$ corresponds to the area in blue, $\psi^*(\hat{\boldsymbol{\sigma}})$ to the area in red, and $\hat{\boldsymbol{\sigma}} : \boldsymbol{\epsilon}(\hat{\mathbf{u}})$ is the area in grey. The residual quantity $\psi(\boldsymbol{\epsilon}(\hat{\mathbf{u}})) + \psi^*(\hat{\boldsymbol{\sigma}}) - \hat{\boldsymbol{\sigma}} : \boldsymbol{\epsilon}(\hat{\mathbf{u}})$ is then the remaining blank area.

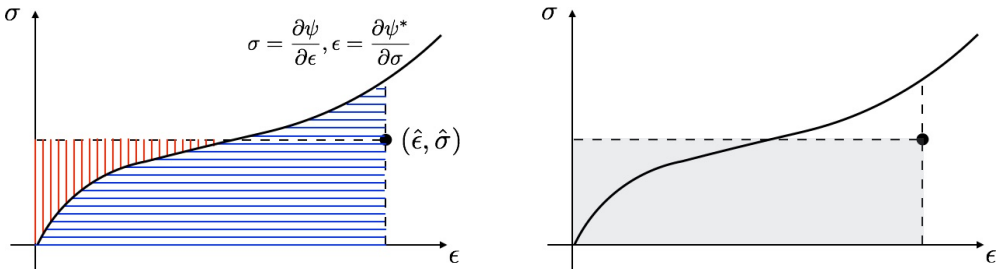

Figure 2: Geometrical representation of the CRE measure for a general elastic behavior.

Let us now define the following error functionals on displacement and stress fields (related to potential and complementary energy functionals):

$$
\begin{aligned}
e_u(\mathbf{e}) &\equiv \int_\Omega \left[\psi(\boldsymbol{\epsilon}(\mathbf{u}+\mathbf{e})) + \psi(\boldsymbol{\epsilon}(\mathbf{u})) - \boldsymbol{\sigma} : \boldsymbol{\epsilon}(\mathbf{u}+\mathbf{e})\right] \mathrm{d}\Omega \quad \forall \mathbf{e} \in [H^1(\Omega)]^d \\
e_\sigma(\mathbb{S}) &\equiv \int_\Omega \left[\psi^*(\boldsymbol{\sigma}+\mathbb{S}) + \psi^*(\boldsymbol{\sigma}) - (\boldsymbol{\sigma}+\mathbb{S}) : \boldsymbol{\epsilon}(\mathbf{u})\right] \mathrm{d}\Omega \quad \forall \mathbb{S} \in [H(div,\Omega)]^d
\end{aligned}
\tag{14}
$$

where $(\mathbf{u}, \boldsymbol{\sigma})$ is the exact solution pair of the elasticity problem. It results that these error functionals and the fully computable CRE functional are interlinked by the following property:

$$
e_u(\hat{\mathbf{u}} - \mathbf{u}) + e_\sigma(\hat{\boldsymbol{\sigma}} - \boldsymbol{\sigma}) = \mathcal{E}^2_{CRE}(\hat{\mathbf{u}}, \hat{\boldsymbol{\sigma}}) \quad \forall (\hat{\mathbf{u}}, \hat{\boldsymbol{\sigma}}) \in \boldsymbol{\mathcal{U}}_{ad} \times \boldsymbol{\mathcal{S}}_{ad} \tag{15}
$$

This property is due to the orthogonality $\int_\Omega (\hat{\boldsymbol{\sigma}} - \boldsymbol{\sigma}) : \boldsymbol{\epsilon}(\hat{\mathbf{u}} - \mathbf{u}) \mathrm{d}\Omega = 0$ coming from admissibility constraints.

Taking $\hat{\mathbf{u}} = \mathbf{u}_h$, the equality (15) is the key to obtain a guaranteed upper bound on a global norm of the discretization error $\mathbf{u}_h - \mathbf{u}$. In the case of linear elasticity for instance, it corresponds to the Prager-Synge equality [145]:

$$
\|\mathbf{u}_h - \mathbf{u}\|^2_{\mathbf{K}} + \|\hat{\boldsymbol{\sigma}} - \boldsymbol{\sigma}\|^2_{\mathbf{K}^{-1}} = \|\hat{\boldsymbol{\sigma}} - \mathbf{K}\boldsymbol{\epsilon}(\mathbf{u}_h)\|^2_{\mathbf{K}^{-1}} = 2.\mathcal{E}^2_{CRE}(\mathbf{u}_h, \hat{\boldsymbol{\sigma}}) \tag{16}
$$

with $\| \bullet \|^2_{\mathbf{K}} \equiv \int_\Omega \boldsymbol{\epsilon}(\bullet) : \mathbf{K}\boldsymbol{\epsilon}(\bullet)\mathrm{d}\Omega$ and $\| \bullet \|^2_{\mathbf{K}^{-1}} \equiv \int_\Omega \bullet : \mathbf{K}^{-1} \bullet \mathrm{d}\Omega$ the energy norms on displacement and stress fields, respectively. This yields the following guaranteed and fully computable upper bounding on the discretization error, provided any stress field $\hat{\boldsymbol{\sigma}} \in \boldsymbol{\mathcal{S}}_{ad}$ is available:

$$\|\mathbf{e}_h\|_{\mathbf{K}} \leq \sqrt{2}\mathcal{E}_{CRE}(\mathbf{u}_h, \hat{\boldsymbol{\sigma}}) \tag{17}$$

Two geometrical representations of the CRE philosophy are now given for linear elasticity (see Fig. 3). The first one, classical, is in the space of stress fields with inner product $\langle \boldsymbol{\sigma}_1, \boldsymbol{\sigma}_2 \rangle \equiv \int_\Omega \boldsymbol{\sigma}_1 : \mathbf{K}^{-1}\boldsymbol{\sigma}_2 \mathrm{d}\Omega$ and associated energy norm. It illustrates the orthogonality property involved in the Prager-Synge equality (16). The distance between $\hat{\boldsymbol{\sigma}}$ and $\boldsymbol{\sigma}_h$, that is $\sqrt{2}.\mathcal{E}_{CRE}(\mathbf{u}_h, \hat{\boldsymbol{\sigma}})$, is an upper error bound on the discretization error $\|\mathbf{u} - \mathbf{u}_h\|_{\mathbf{K}}$.
The second one, not classical but that will be later reused, is in the space of strain-stress couples $s = (\boldsymbol{\epsilon}, \boldsymbol{\sigma})$. This space is equipped with the energy inner product $\langle s_1, s_2 \rangle \equiv \int_\Omega (\boldsymbol{\epsilon}_1 : \mathbf{K}\boldsymbol{\epsilon}_2 + \boldsymbol{\sigma}_1 : \mathbf{K}^{-1}\boldsymbol{\sigma}_2)\mathrm{d}\Omega$ and associated energy norm. We denote $(\mathbf{A}_d)$ the space of (kinematically and statically) admissible couples, and $\boldsymbol{\Gamma}$ the space (linear here) associated with the constitutive law. The exact solution of the well-posed problem (1)-(3) is defined by the intersection between $(\boldsymbol{\Gamma})$ and $(\mathbf{A}_d)$. It is then easy to show that the value $\mathcal{E}_{CRE}$ exactly corresponds to the distance from the solution $\hat{s} = (\boldsymbol{\epsilon}(\mathbf{u}_h), \hat{\boldsymbol{\sigma}}) \in (\mathbf{A}_d)$ at hand to $(\boldsymbol{\Gamma})$, with orthogonal projection. The stress field $\boldsymbol{\sigma}_m$ obtained after projection is the average field $\boldsymbol{\sigma}_m = \frac{1}{2}(\hat{\boldsymbol{\sigma}} + \boldsymbol{\sigma}_h)$. The Prager-Synge theorem reads in this framework:

$$\langle s - \hat{s}, s - \hat{s} \rangle = 2.\mathcal{E}^2_{CRE}(\hat{s})$$

and $\langle s-\hat{s}, s-\hat{s} \rangle$ is the squared of the distance to the exact solution represented in red in Fig. 3.

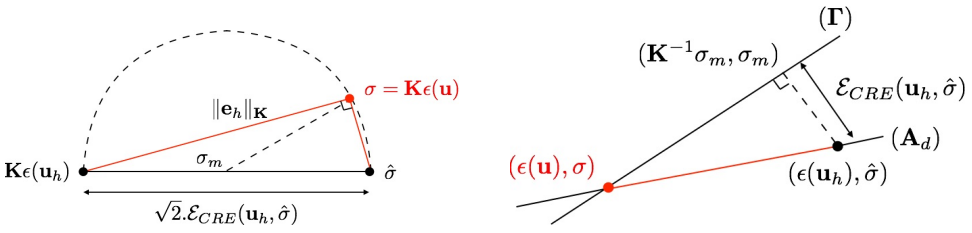

Figure 3: Geometrical representations of the CRE concept.

2.3. Practical computation of admissible fields

The quality of the bounding derived from the CRE (e.g., (17)) depends on that of the statically admissible stress field $\hat{\boldsymbol{\sigma}}$ at hand. The suitable construction of such a fully equilibrated stress field is actually the key and technical point of the CRE concept; it may be addressed by means of various techniques available in the literature. A natural one is to approximately solve in parallel the dual elasticity problem by means of equilibrium elements which enforce equilibrium by construction [47, 69, 89, 124]. This provides for the sharpest error bounds in practice, but it requires the use of specific approximation functions with challenging implementation in commercial finite element software (since it refers to a non-conventional numerical architecture) out of solving an additional global problem with large computational effort.

Alternative techniques rather aim at post-processing the FE solution at hand, as the approximate stress field $\boldsymbol{\sigma}_h$ already satisfies some weak equilibrium properties (in the FE sense). These techniques usually involve local independent computations over the FE mesh. Let us mention:

- the hybrid-flux technique also known as Element Equilibration Technique (EET), initially developed in [93, 97], which is quasi-explicit. It consists in constructing equilibrated tractions on element edges, before solving local problems at the element level over the FE mesh. Several variants of this technique were proposed over the years [98, 67, 111, 144, 159, 27, 4] to improve performance or easiness of implementation;

- flux-free techniques developed in [138, 45, 72, 123, 139], which are simpler to analyze and implement than the hybrid-flux technique as they circumvent the need to construct equilibrated tractions on element edges. Nevertheless, they require to solve local problems over patches of elements and are therefore more expensive [40];

- techniques based on a mixed formulation and the use of Raviart-Thomas-Nédélec (RTN) elements [53, 118, 157, 60, 61].

We refer to [33] for more details on all these techniques, and to [143] for a comparative analysis of performance of some of them on engineering examples.

Remark 3. *It can be shown that using the hybrid-flux (or EET) technique to construct $\hat{\boldsymbol{\sigma}}$, a lows error bound is also available from the CRE functional [93, 33]; it is of the form $\mathcal{E}_{CRE}(\mathbf{u}_h, \hat{\boldsymbol{\sigma}}) \leq C\|\mathbf{u}_h - \mathbf{u}\|$ where C is a constant independent of the mesh size, and it sproves that the constructed error estimate has the same convergence rate as the true discretization error. A lower bound can also be obtained using a mixed formulation with RTN elements.*

Remark 4. *We also mention that $\mathbf{u}_h$ is usually chosen as the kinematically admissible field $\hat{\mathbf{u}}$ in* (15)*. Nevertheless, in the case of quasi-incompressible materials with additional kinematic constraints, a correction should be brought to $\mathbf{u}_h$ to ensure admissibility [95].*

2.4. Illustrative example

We report here a numerical experiment taken from [143]. A linear elasticity problem, with isotropic and homogeneous material behavior, is considered on a three-dimensional physical domain (which represents the hub of the main rotor of an helicopter). The mechanical structure is clamped on part of its boundary, and is subjected to unit tractions $\boldsymbol{t}$, normal to the boundary surface, on another part of its boundary. The considered geometry and mesh, made of 1978 linear tetrahedral elements (17,694 dofs), are shown in Fig. 4.

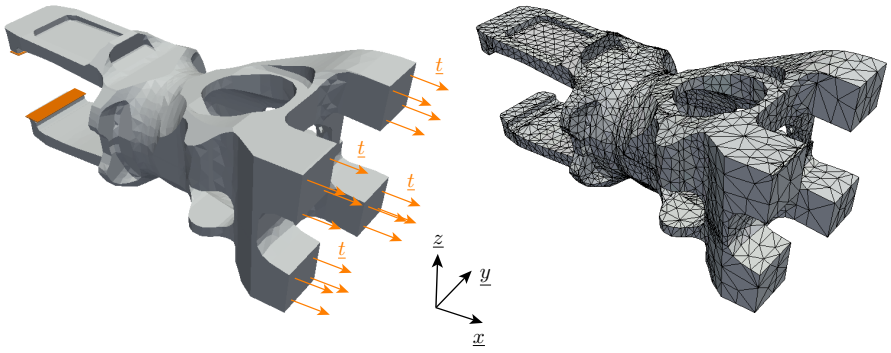

Figure 4: Model problem (left) and associated FE mesh (right). Colored planes represent clamped boundary parts.

A conforming FEM is used to compute an approximate solution $\mathbf{u}_h$. In this example, a selected region of the structure plays an essential role for

design purposes and engineering interest. The magnitude (with Frobenius norm) of the FE stress field in this region is shown in Fig. 5.

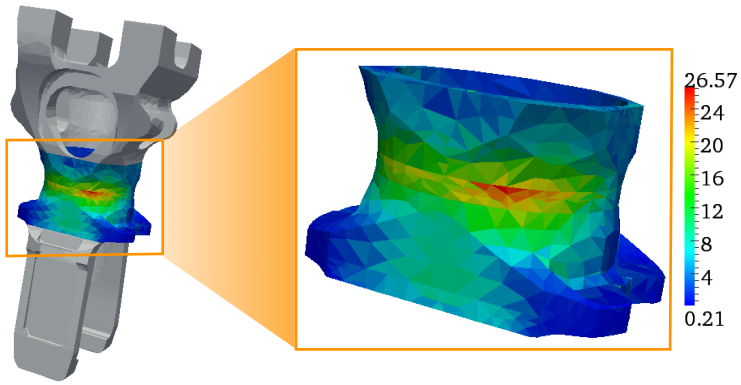

Figure 5: Magnitude of the FE stress field in the selected region of interest.

A posteriori error estimation is then performed using the presented CRE concept and bound (17). The magnitude of the admissible stress field $\hat{\boldsymbol{\sigma}}$, obtained using a hybrid-flux equilibration technique as a post-processing of $\boldsymbol{\sigma}_h$, as well as the spatial distribution of the obtained CRE error estimate $\sqrt{2}.\mathcal{E}_{CRE}(\mathbf{u}_h, \hat{\boldsymbol{\sigma}})$, are shown on Fig. 6.

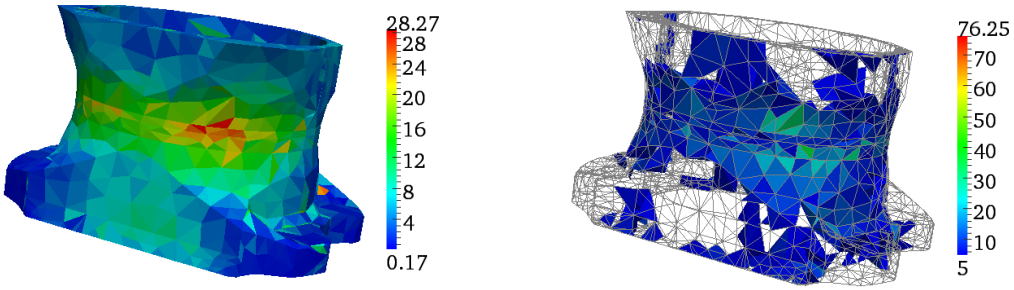

Figure 6: Magnitude of the admissible stress field (left), and spatial distribution of relevant local contributions to the error estimate (right).

2.5. Extension to complex nonlinear mechanics problems

We now extend the CRE concept to dissipative material behaviors with standard formulation involving internal variables [81, 74], such as viscoplas-

ticity. For the sake of conciseness, we use some global notations to handle all mechanical quantities. We thus introduce the following generalized quantities:

$$\mathbf{s} = \begin{bmatrix} \boldsymbol{\varpi} \\ \mathbf{Y} \end{bmatrix} \qquad \mathbf{e}_e = \begin{bmatrix} \boldsymbol{\epsilon}_e \\ \mathbf{X} \end{bmatrix} \qquad \mathbf{e}_p = \begin{bmatrix} \boldsymbol{\epsilon}_p \\ -\mathbf{X} \end{bmatrix} \qquad \mathbf{e} = \mathbf{e}_e + \mathbf{e}_p \tag{18}$$

where $\boldsymbol{\epsilon}_e$ (resp. $\boldsymbol{\epsilon}_p$) denotes the elastic (resp. plastic) part of the strain tensor, vector $\mathbf{X}$ gathers additional internal variables, and vector $\mathbf{Y}$ gathers the associated thermodynamic forces. The local dissipation then reads:

$$d = \boldsymbol{\varpi} : \dot{\boldsymbol{\epsilon}}_p - \mathbf{Y} \cdot \dot{\mathbf{X}} = \mathbf{s} \cdot \dot{\mathbf{e}}_p \tag{19}$$

where $\mathbf{y} \cdot \mathbf{x}$ denotes the duality product between variables $\mathbf{x}$ and $\mathbf{y}$.

In this thermodynamic framework, two pairs (ψ, ψ^*) and (φ, φ^*) of conjugate convex potentials (defined from the Legendre-Fenchel transform) are introduced; they describe the two complementary parts of the overall material behavior:

- state equations:

$$\mathbf{e}_e = \Lambda(\mathbf{s}) = \frac{\partial \psi^*}{\partial \mathbf{s}} \quad (\text{or } \mathbf{s} = \frac{\partial \psi}{\partial \mathbf{e}_e}) \tag{20}$$

- evolution laws:

$$\dot{\mathbf{e}}_p = \mathbf{B}(\mathbf{s}) = \frac{\partial \varphi^*}{\partial \mathbf{s}} \quad (\text{or } \mathbf{s} = \frac{\partial \varphi}{\partial \dot{\mathbf{e}}_p}) \tag{21}$$

In practice, the potential ψ refers to the Helmholtz free energy, while φ is a convex non-negative dissipation potential ensuring stability conditions.

Remark 5. *When φ^* is not differentiable at some points (usual case in elasto-plasticity), the evolution laws should be replaced by $\dot{\mathbf{e}}_p \in \partial_{\mathbf{s}} \varphi^*$ where $\partial_{\mathbf{s}} \varphi^*$ denotes the sub-differential of φ^* defined as:*

$$\partial_{\mathbf{s}} \varphi^* \equiv \{\dot{\mathbf{e}}_p \textit{ such that } \varphi^*(\overline{\mathbf{s}}) - \varphi^*(\mathbf{s}) \geq \dot{\mathbf{e}}_p \cdot (\overline{\mathbf{s}} - \mathbf{s}) \quad \forall \overline{\mathbf{s}}\} \tag{22}$$

Considering an admissible solution $(\hat{\mathbf{e}}_e, \hat{\mathbf{e}}_p, \hat{\mathbf{s}})$ over the space-time domain $\Omega \times [0,T]$, with $\hat{\mathbf{e}}_e + \hat{\mathbf{e}}_p = \hat{\mathbf{e}}$, residuals on these two parts (20) and (21) are naturally defined in a similar way as in Eq. (11):

$$\eta_\psi(\hat{\mathbf{e}}_e, \hat{\mathbf{s}}) = \psi(\hat{\mathbf{e}}_e) + \psi^*(\hat{\mathbf{s}}) - \hat{\mathbf{s}} \cdot \hat{\mathbf{e}}_e \quad ; \quad \eta_\varphi(\dot{\hat{\mathbf{e}}}_p, \hat{\mathbf{s}}) = \varphi(\dot{\hat{\mathbf{e}}}_p) + \varphi^*(\hat{\mathbf{s}}) - \hat{\mathbf{s}} \cdot \dot{\hat{\mathbf{e}}}_p \quad (23)$$

Residuals η_ψ and η_φ are here local in space and time quantities. The following CRE measure is then introduced at time $t \in [0,T]$ [101]:

$$\mathcal{E}^2_{CRE|t}(\hat{\mathbf{e}}, \hat{\mathbf{s}}) = \int_\Omega \eta_\psi(\hat{\mathbf{e}}_e, \hat{\mathbf{s}}) \mathrm{d}\Omega + \int_0^t \int_\Omega \eta_\varphi(\dot{\hat{\mathbf{e}}}_p, \hat{\mathbf{s}}) \mathrm{d}\Omega \, \mathrm{d}\tau \geq 0 \qquad (24)$$

This CRE measure vanishes when $(\hat{\mathbf{e}}, \hat{\mathbf{s}})$ corresponds to the exact solution of the problem. In other cases, it integrates error sources coming from space and time discretizations, as well as iteration stopping, and it can be linked to the exact error (see [99, 105, 115] for details).

Remark 6. *An alternative definition of the CRE measure, known as the dissipation error [99], consists in integrating state equations in admissibility conditions (so that $\hat{\mathbf{e}}_p = \hat{\mathbf{e}} - \Lambda(\hat{\mathbf{s}})$), and to measure the residual on evolution laws alone.*

The construction of an admissible solution can again be conducted from the approximate solution $(\mathbf{e}_h, \mathbf{s}_h)$ given by the FE method, and known at discrete time points t_n (with kinematic constraints and weak FE equilibrium satisfied at these time points). This approximate solution is first extended across the whole time-space domain, in order to satisfy kinematic constraints and weak FE equilibrium at any time $t \in [0,T]$, then an equilibration technique similar to those defined for the elasticity case (see Section 2.3) is used to compute an admissible solution $(\hat{\mathbf{e}}, \hat{\mathbf{s}})$. Let us note that admissible additional internal variables $(\hat{\mathbf{X}}, \hat{\mathbf{Y}})$ can be easily constructed by solving local problems related to the minimization of the CRE functional. All details on this construction of an admissible solution can be found in [99, 102, 105].

2.6. Extension to the control of PGD reduced order modeling

Reduced order modeling (ROM) has received a growing interest and has been an active research topic over the last 20 years [38], in particular to efficiently address parameterized models associated with multi-query simulations such as encountered in inverse analysis, uncertainty propagation, or

optimization. ROM circumvents the curse of dimensionality, that is the exponential increase in the number of dofs with respect to the number of parameters, that rapidly leads to unaffordable computations when using brute-force numerical methods. Among the list of ROM techniques, the Proper Generalized Decomposition (PGD) appears very attractive in many engineering applications (see [37] for a review). It is based on a modal representation of the solution, defined as a linear combination of separated variable functions (modes); variables include space, time, but also parameters seen as extra-coordinates of the problem and related to geometry, material properties, loading, boundary or initial conditions, etc. This representation (i.e., low-rank canonical format approximation) reads:

$$\mathbf{u}_{PGD}(\mathbf{x}, t, \mathbf{p}) = \sum_{m=1}^{M} \mathbf{X}_m(\mathbf{x}).T_m(t).\Pi_{k=1}^{K}\zeta_{k,m}(p_k) \tag{25}$$

where $\mathbf{p} = [p_1, p_2, \ldots, p_K]^T$ is the vector of parameters. PGD modes are computed in an offline phase, then the obtained PGD approximation (which explicitly depends on model parameters) can be used in the online phase with cheap and fast evaluation on light computing platforms. This makes the approximation of high-dimensional solutions computationally tractable. A main concern in the use of PGD reduced models is to assess their reliability, that is to control the accuracy of PGD outputs. This requires to adaptively set the number M of modes which have to be computed in the truncated sum (25), as well as the discretization technique (mesh and time step sizes) used to compute these modes. For this purpose, a robust approach for the verification of PGD models was designed using the CRE concept in [112]. It provides for quantitative error bounds, as well as indicators on contributions of the various error sources (that are space/time discretizations and truncation of the PGD representation) to drive a greedy adaptive algorithm. The approach is based on a specific processing of the approximate PGD solution at hand in order to construct admissible fields over the whole parametric domain. Performances were shown in [112, 25, 3, 28] on some numerical experiments exhibiting various situations in terms of models and hyper-parameters.

We report here an illustration taken from [30] and dealing with the coupled use of IGA and PGD to effectively simulate problems with parameterized geometry, for shape optimization purposes. An elasticity problem is considered over a plate with a hole at the center, and submitted to a biaxial

traction loading (Fig. 7). The material is supposed to be linear and isotropic, the plane stress assumption is made, and only a quarter of the plate is studied due to symmetry conditions. The hole radius R is chosen as a geometrical parameter, with $R \in [1, 2]$. The geometry is represented with NURBS functions (see the control mesh in Fig. 7), and its parametrization is defined by means of a mapping from the IGA parametric space to the physical space. Parameters are then related to the coordinates and weights of control points defined at the coarsest-mesh level used to represent the geometry (Fig. 8).

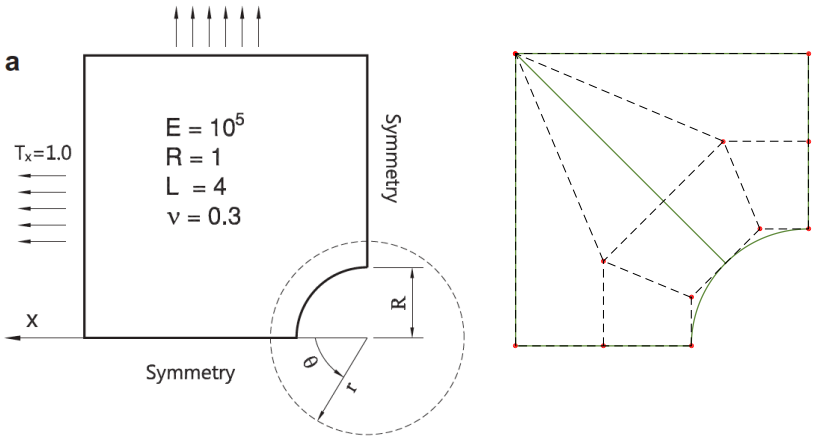

Figure 7: Definition of the elasticity problem on the holed plate (left), and IGA representation of the geometry (right).

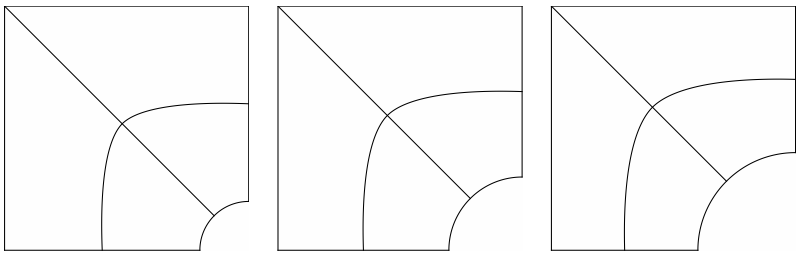

Figure 8: Configuration of the initial coarse IGA mesh for different values of R.

PGD model reduction is then performed with a separation between space and geometry variables; the first three PGD modes in space and in geometry parameters are displayed in Fig. 9 and Fig. 10, respectively.

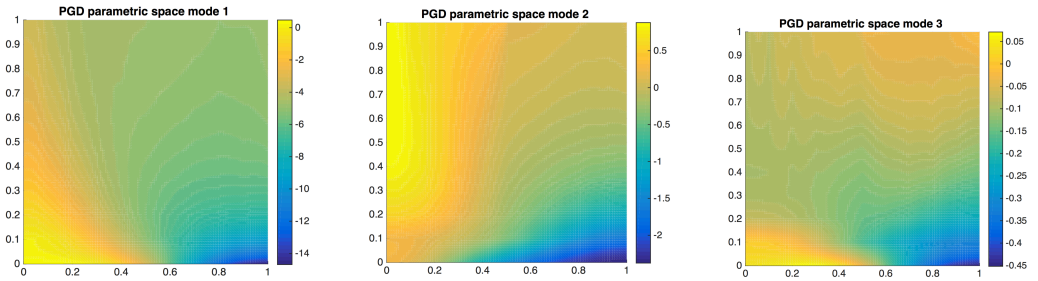

Figure 9: First three PGD modes in space (from left to right) in the IGA parametric space $\overline{\Omega}$.

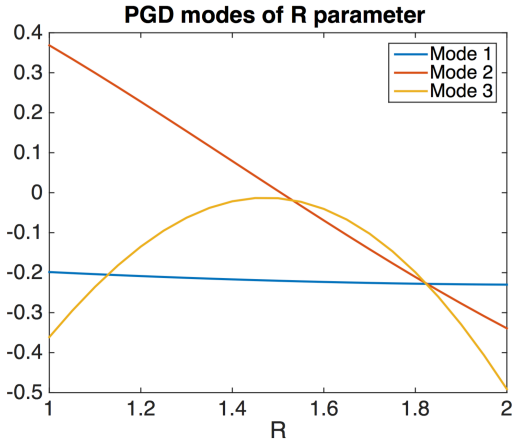

Figure 10: First three PGD modes in parameter R.

Using the PGD enables to describe the resulting manifold of parametric solutions with reduced CPU cost (e.g., the PGD solution evaluated for $R \in \{1, 1.5, 2\}$ is shown in Fig. 11). Therefore, virtual charts can be built for shape optimization, with explicit and continuous dependency of the solution to design variables.

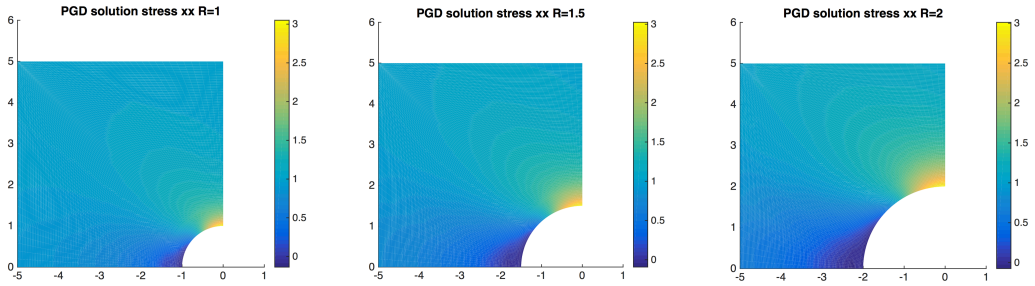

Figure 11: Approximate 3-mode PGD solution for various values of R.

In this framework, a posteriori error estimation is conducted from CRE to quantitatively assess error sources (discretization & truncation), control the quality of the approximate PGD solution (for any geometry in the design domain) with guaranteed error bounds, and feed an adaptive algorithm that optimizes the computational effort and memory space for a prescribed accuracy. The CRE-based approach involves the implementation of the hybrid-flux equilibration technique developed for IGA in [156]. After computing the first PGD mode, the evolution of the global error estimate $\mathcal{E}_{CRE}(\mathbf{u}_{PGD}(\cdot,\mathbf{p}),\hat{\boldsymbol{\sigma}}_{\mathbf{p}})$ with respect to R is reported in Fig. 12. It shows that the highest error level is made for the smallest value $R=1$. Results of the adaptive process are also given in Fig. 12. They indicate that mesh refinements are necessary when computing PGD modes 4 and 5.

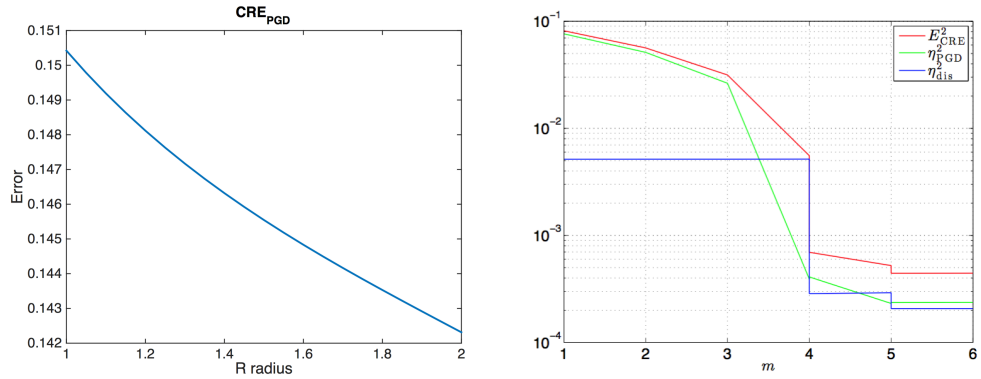

Figure 12: Evolution of the estimate $\mathcal{E}_{CRE}(\mathbf{u}_{PGD}(\cdot,\mathbf{p}),\hat{\boldsymbol{\sigma}}_{\mathbf{p}})$ with respect to R after computing the first PGD mode (left), and evolution of error estimator (in red) and indicators on PGD error (in green) and discretization error (in blue) along the greedy adaptive process (right).

3. Goal-oriented error estimation with the CRE concept

In this section, we present some of the advances performed in the last 20 years for goal-oriented error estimation, that is estimation of the discretization error on local quantities of interest, with the CRE concept. They mainly concern technical points, and various applications to engineering problems.

3.1. Quantity of interest and adjoint problem

For the sake of clarity, we first deal with a linear elasticity problem with constitutive relation given by (9). We consider a quantity of interest Q which is a linear continuous functional of $\mathbf{u}$ (e.g., local average of a displacement or stress component). It is written under the following global form:

$$Q(\mathbf{u}) = \int_\Omega \left(\tilde{\boldsymbol{\varpi}}_\Sigma : \boldsymbol{\epsilon}(\mathbf{u}) + \tilde{\mathbf{f}}_\Sigma \cdot \mathbf{u} \right) \mathrm{d}\Omega + \int_{\partial_2\Omega} \tilde{\mathbf{F}}_\Sigma \cdot \mathbf{u} \mathrm{d}S \tag{26}$$

where $(\tilde{\boldsymbol{\varpi}}_\Sigma, \tilde{\mathbf{f}}_\Sigma, \tilde{\mathbf{F}}_\Sigma)$ are extraction functions which define Q; they correspond to pre-stress, body force, and tractions, respectively, and they are defined explicitly or implicitly.

The objective is to assess the discretization error on Q, that is $Q(\mathbf{u}_h) - Q(\mathbf{u})$. For this, and to get a relevant error bound, a classical practice is to refer to the adjoint problem with displacement-stress solution pair $(\tilde{\mathbf{u}}, \tilde{\boldsymbol{\varpi}})$. In the present case, the adjoint problem remains an elasticity problem loaded with $(\tilde{\boldsymbol{\varpi}}_\Sigma, \tilde{\mathbf{f}}_\Sigma, \tilde{\mathbf{F}}_\Sigma)$, and with homogeneous Dirichlet boundary conditions on $\partial_1\Omega$ ($\tilde{\mathbf{u}} \in \boldsymbol{\mathcal{U}}_{ad,0}$). The weak form of adjoint equilibrium equations reads:

$$\int_\Omega \tilde{\boldsymbol{\varpi}} : \boldsymbol{\epsilon}(\mathbf{v}) \mathrm{d}\Omega = Q(\mathbf{v}) = \int_\Omega \left(\tilde{\boldsymbol{\varpi}}_\Sigma : \boldsymbol{\epsilon}(\mathbf{v}) + \tilde{\mathbf{f}}_\Sigma \cdot \mathbf{v} \right) \mathrm{d}\Omega + \int_{\partial_2\Omega} \tilde{\mathbf{F}}_\Sigma \cdot \mathbf{v} \mathrm{d}S \quad \forall \mathbf{v} \in \boldsymbol{\mathcal{U}}_{ad,0} \tag{27}$$

We assume that an approximate adjoint solution $(\tilde{\mathbf{u}}_h, \tilde{\boldsymbol{\varpi}}_h)$ is computed from FEM (with a possibly different mesh compared to the one used for primal approximate elasticity solution), and that a statically admissible field $\hat{\tilde{\boldsymbol{\varpi}}}$ satisfying (27) is recovered using one of the techniques defined in Section 2.3.

3.2. CRE-based error bound

In order to get a goal-oriented error bound from the CRE, we use the following hypercircle property:

$$\mathcal{E}^2_{CRE}(\mathbf{u}_h, \hat{\boldsymbol{\varpi}}) = 2\|\boldsymbol{\varpi} - \hat{\boldsymbol{\varpi}}^m\|^2_{\mathbf{K}^{-1}} \quad \text{with } \hat{\boldsymbol{\varpi}}^m = \frac{1}{2}(\hat{\boldsymbol{\varpi}} + \boldsymbol{\varpi}_h) \tag{28}$$

which is a direct consequence of the Prager-Synge equality (16). It then yields:

$$\begin{aligned} Q(\mathbf{u}) - Q(\mathbf{u}_h) &= \int_\Omega \tilde{\boldsymbol{\sigma}} : \boldsymbol{\epsilon}(\mathbf{u} - \mathbf{u}_h) \mathrm{d}\Omega \\ &= \int_\Omega \hat{\tilde{\boldsymbol{\sigma}}} : \boldsymbol{\epsilon}(\mathbf{u} - \mathbf{u}_h) \mathrm{d}\Omega \\ &= \int_\Omega (\hat{\tilde{\boldsymbol{\sigma}}} - \mathbf{K}\boldsymbol{\epsilon}(\tilde{\mathbf{u}}_h)) : \boldsymbol{\epsilon}(\mathbf{u} - \mathbf{u}_h) \mathrm{d}\Omega + \int_\Omega \boldsymbol{\epsilon}(\tilde{\mathbf{u}}_h) : (\boldsymbol{\sigma} - \boldsymbol{\sigma}_h) \mathrm{d}\Omega \\ &= \int_\Omega (\hat{\tilde{\boldsymbol{\sigma}}} - \mathbf{K}\boldsymbol{\epsilon}(\tilde{\mathbf{u}}_h)) : \mathbf{K}^{-1}(\boldsymbol{\sigma} - \boldsymbol{\sigma}_h) \mathrm{d}\Omega + \int_\Omega \boldsymbol{\epsilon}(\tilde{\mathbf{u}}_h) : (\hat{\boldsymbol{\sigma}} - \boldsymbol{\sigma}_h) \mathrm{d}\Omega \\ &= \int_\Omega (\hat{\tilde{\boldsymbol{\sigma}}} - \mathbf{K}\boldsymbol{\epsilon}(\tilde{\mathbf{u}}_h)) : \mathbf{K}^{-1}(\boldsymbol{\sigma} - \hat{\boldsymbol{\sigma}}^m) \mathrm{d}\Omega + Q_{corr} \end{aligned} \tag{29}$$

where

$$\begin{aligned} Q_{corr} &= \int_\Omega (\hat{\tilde{\boldsymbol{\sigma}}} - \mathbf{K}\boldsymbol{\epsilon}(\tilde{\mathbf{u}}_h)) : \mathbf{K}^{-1}(\hat{\boldsymbol{\sigma}}^m - \boldsymbol{\sigma}_h) \mathrm{d}\Omega + \int_\Omega \boldsymbol{\epsilon}(\tilde{\mathbf{u}}_h) : (\hat{\boldsymbol{\sigma}} - \boldsymbol{\sigma}_h) \mathrm{d}\Omega \\ &= \frac{1}{2} \int_\Omega (\hat{\tilde{\boldsymbol{\sigma}}} + \mathbf{K}\boldsymbol{\epsilon}(\tilde{\mathbf{u}}_h)) : \mathbf{K}^{-1}(\hat{\boldsymbol{\sigma}} - \boldsymbol{\sigma}_h) \mathrm{d}\Omega \end{aligned} \tag{30}$$

is a computable correction term. Consequently, from the Cauchy-Schwarz inequality and the property (28), a fully computable CRE-based upper error bound is obtained [107]:

$$\begin{aligned} |Q(\mathbf{u}) - Q(\mathbf{u}_h) - Q_{corr}| &\leq \|\boldsymbol{\sigma} - \hat{\boldsymbol{\sigma}}^m\|_{\mathbf{K}^{-1}} . \|\hat{\tilde{\boldsymbol{\sigma}}} - \mathbf{K}\boldsymbol{\epsilon}(\tilde{\mathbf{u}}_h)\|_{\mathbf{K}^{-1}} \\ &\leq \mathcal{E}_{CRE}(\mathbf{u}_h, \hat{\boldsymbol{\sigma}}) . \mathcal{E}_{CRE}(\tilde{\mathbf{u}}_h, \hat{\tilde{\boldsymbol{\sigma}}}) \end{aligned} \tag{31}$$

The quantity $Q(\mathbf{u}_h) + Q_{corr}$ can be interpreted as a corrected approximate value of the quantity of interest $Q(\mathbf{u})$. Furthermore, the estimate (31) can also be written as:

$$|Q(\mathbf{u}) - Q(\mathbf{u}_h)| \leq \max_{\theta=\pm 1} |Q_{corr} + \theta . \mathcal{E}_{CRE}(\mathbf{u}_h, \hat{\boldsymbol{\sigma}}) . \mathcal{E}_{CRE}(\tilde{\mathbf{u}}_h, \hat{\tilde{\boldsymbol{\sigma}}})| \tag{32}$$

Remark 7. *The value of the calculated error bound depends on the meshes used to solve the reference and adjoint problems. It is always possible, by refining the mesh of the adjoint problem alone, to control the value of the error on Q. In general, a local refinement (near the domain of interest) of the mesh used to solve the adjoint problem is very effective [23, 136].*

Remark 8. *The bound* (31) *is based on the Cauchy-Schwarz inequality as nearly all error bounds, and this may give a crude upper bound as its does not take spatial locality into account. In [114], a new bounding technique using the Saint-Venant principle and homothetic domains was derived, giving sharper bounds. The idea is to decompose the domain* Ω *in two disjoint zones: (i) zone* ω_λ*, parameterized with scalar value* λ*, surrounding the zone where the quantity of interest is defined; (ii) complementary zone* Ω/ω_λ*. We can then write* $Q(\mathbf{u}) - Q(\mathbf{u}_h) - Q_{corr} = q_{\omega_\lambda} + q_{\Omega/\omega_\lambda}$*.*
Bounding the term $q_{\Omega/\omega_\lambda}$ *can be easily and accurately performed from the Cauchy-Schwarz inequality applied over* Ω/ω_λ*, as* $\tilde{\mathcal{E}}_{CRE|\Omega/\omega_\lambda}$ *remains small in practice. Bounding the other term* q_{ω_λ} *is more technical; it leans on an inequality, related to Saint-Venant's principle, of the form:*

$$||\boldsymbol{\sigma} - \hat{\boldsymbol{\sigma}}_h||_{\mathbf{K}^{-1}|\omega_\lambda} \leq (\frac{\lambda}{\overline{\lambda}})^{1/k} ||\boldsymbol{\sigma} - \hat{\boldsymbol{\sigma}}_h||_{\mathbf{K}^{-1}|\omega_{\overline{\lambda}}} + \gamma_{\lambda,\overline{\lambda}} \tag{33}$$

where $\omega_{\overline{\lambda}}$ *is a homothetic domain of* ω_λ*, parameterized by scalar value* $\overline{\lambda} \geq \lambda$ *(Fig. 13),* k *is a computable (Steklov) constant that depends on the geometry of* ω_λ *(and obtained analytically or numerically by solving an additional local eigenvalue problem), and* $\gamma_{\lambda,\overline{\lambda}}$ *is a known term. In practice,* $\overline{\lambda}$ *is chosen the highest possible while ensuring* $\omega_{\overline{\lambda}} \subset \Omega$*, and* λ *the smallest possible with* ω_λ *surrounding the zone of interest. The exponential decrease with respect to* $\lambda/\overline{\lambda}$ *in* (33) *is the key point to avoid overestimation.*

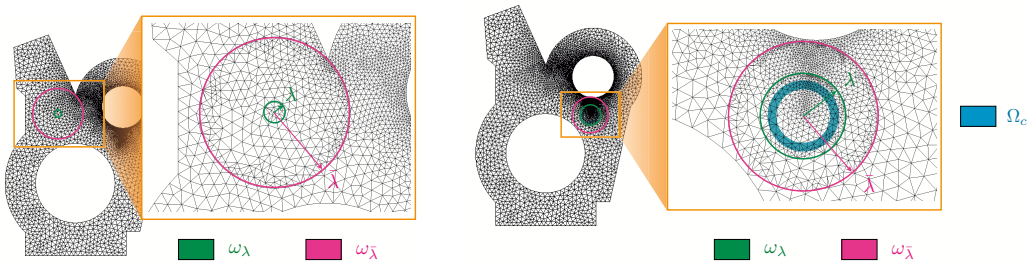

Figure 13: Homothetic domains ω_λ and $\omega_{\overline{\lambda}}$ defined in a cracked structure when considering different quantities of interest: local mean of a component of $\boldsymbol{\sigma}$ (left), and stress intensity factors in the vicinity of the crack (right).

3.3. Numerical illustration

To illustrate the performance of the CRE-based goal-oriented error estimation approach, we again consider the numerical example described in

Section 2.4, but now focusing on the accuracy on a specific quantity of interest. It is chosen as the average, over a critical three-dimensional subdomain ω of the structure, of the zz component of the stress tensor (z is the axial direction of the structure): $Q(\mathbf{u}) = \frac{1}{|\omega|}\int_\omega \sigma_{zz}(\mathbf{u})\mathrm{d}\omega$. The subdomain ω is shown in Fig. 14 and includes about 15 finite elements.

The reference value of the quantity of interest (computed using a very fine mesh) is $Q(\mathbf{u}) = 33.24$. Using FEM, we obtain the approximate value $Q(\mathbf{u}_h) = 28.18$. To obtain a bound on $Q(\mathbf{u}) - Q(\mathbf{u}_h)$, we implement the bounding (31) with refined mesh for the adjoint problem. It yields that the exact value $Q(\mathbf{u})$ satisfies $31.17 \leq Q(\mathbf{u}) \leq 34.29$ (the correction term Q_{corr} is such that $Q(\mathbf{u}_h) + Q_{corr} = 32.73$). We observe that the actual exact value indeed satisfies these bounds, and that the lower (resp., upper) bound underestimates (resp., overestimates) the exact value of Q by only 6% (resp., 3%). The bound thus yields a very accurate estimate.

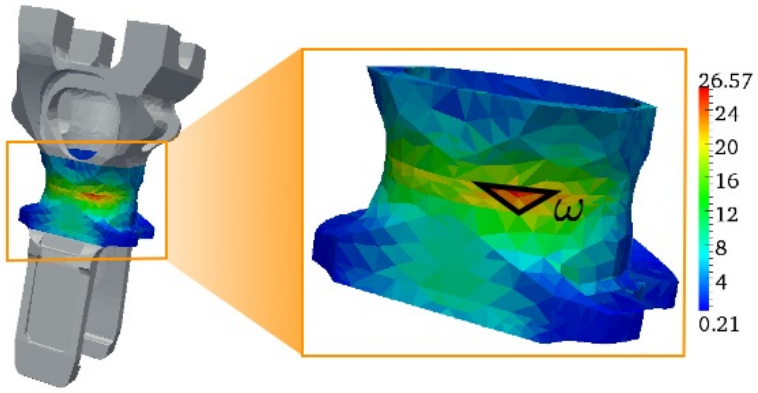

Figure 14: Representation of the subdomain of interest ω. The value of the stress field (in the Frobenius norm) in the neighborhood of ω is indicated.

3.4. Non-intrusive approach

As noticed before, the accuracy of the error bounds on Q can be controlled solving the adjoint problem with a locally refined mesh. However, this has the drawback to require remeshing. An alternative, qualified as non-intrusive as the initial mesh is not changed, was proposed in [24, 110]. It consists in a local enrichment of the adjoint solution, using a Partition of Unity Method (PUM), with known handbook functions that aim at representing the high

gradient part of $(\tilde{\mathbf{u}}, \tilde{\boldsymbol{\varpi}})$. The approach is thus similar to that proposed in XFEM or GFEM except that no additional dof is introduced here (the singularity comes from the adjoint loading). We present the method in the linear elasticity case, but extensions to time-dependent problems can also be found in [24, 158].

The enrichment functions which are used, denoted $(\tilde{\mathbf{u}}^{hand}, \tilde{\boldsymbol{\varpi}}^{hand})$ in the following, correspond to generalized Green's functions and represent the (quasi-)exact adjoint solution in a (semi-)infinite domain subjected to the adjoint loading. These functions are obtained either analytically or pre-computed numerically with a fine mesh and sufficiently large domain. An example of such a function, corresponding to a localized pre-stress loading $\tilde{\boldsymbol{\varpi}}_{\Sigma}$, is given in Fig. 15.

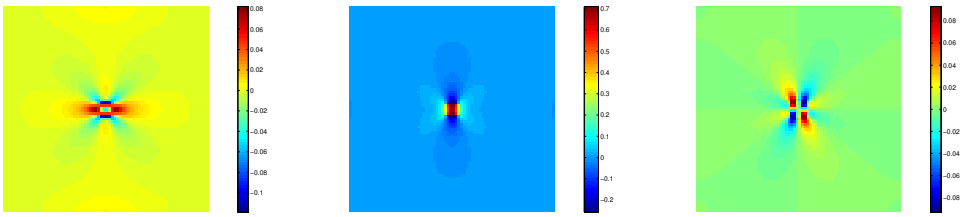

Figure 15: Quasi-exact stress field in a (quasi-) infinite domain subjected to a local pre-stress in a squared region: $\tilde{\boldsymbol{\varpi}}_{xx}^{hand}$ (left), $\tilde{\boldsymbol{\varpi}}_{yy}^{hand}$ (center), $\tilde{\boldsymbol{\varpi}}_{xy}^{hand}$ (right).

Handbook functions are inserted in the adjoint solution using the partition of unity defined by linear FE shape functions N_i associated to vertices i of the initial mesh ($N_i(\mathbf{x}_j) = \delta_{ij}$). The enrichment is introduced locally, and consequently only a set of n^{PUM} vertices is used. The enrichment region $\Omega^{PUM} \subset \Omega$ is defined as $\{\mathbf{x} \in \Omega, \sum_{i=1}^{n^{PUM}} N_i(\mathbf{x}) \neq 0\}$; it can be divided in two disjoint subregions Ω_1^{PUM} and Ω_2^{PUM} such that:

$$\sum_{i=1}^{n^{PUM}} N_i(\mathbf{x}) = \begin{cases} 1 & \text{in } \Omega_1^{PUM} \\ a \in]0,1[& \text{in } \Omega_2^{PUM} \\ 0 & \text{in } \Omega / (\overline{\Omega_1^{PUM} \cup \Omega_2^{PUM}}) \end{cases} \tag{34}$$

In practice, Ω_1^{PUM} is such that it contains the zone of interest Ω_{Σ} in which the quantity Q is defined, i.e. the region that supports extraction functions.

Therefore, the displacement solution to the adjoint problem is searched under the form:

$$\tilde{\mathbf{u}}(\mathbf{x}) = \sum_{i=1}^{n^{PUM}} \tilde{\mathbf{u}}^{hand}(\mathbf{x}) N_i(\mathbf{x}) + \tilde{\mathbf{u}}^{res}(\mathbf{x}) \tag{35}$$

where $\tilde{\mathbf{u}}^{res}$ is a residual solution, usually very regular, to be computed. The enrichment part $\sum_{i=1}^{n^{PUM}} \tilde{\mathbf{u}}^{hand} N_i$ enables to reproduce local high gradients of $\tilde{\mathbf{u}}$ whereas the residual part $\tilde{\mathbf{u}}^{res}$ enables to correct the enrichment part in order to satisfy boundary conditions of the adjoint problem on $\partial\Omega$. The new expression of $\tilde{\boldsymbol{\sigma}}$ is deducted from (35):

$$\tilde{\boldsymbol{\sigma}}(\mathbf{x}) = \tilde{\boldsymbol{\sigma}}^{hand}_{PUM}(\mathbf{x}) + \tilde{\boldsymbol{\sigma}}^{res}(\mathbf{x}) \tag{36}$$

with $\tilde{\boldsymbol{\sigma}}^{hand}_{PUM} = \mathbf{K}\boldsymbol{\epsilon}(\sum_{i=1}^{n^{PUM}} \tilde{\mathbf{u}}^{hand} N_i)$, and $\tilde{\boldsymbol{\sigma}}^{res} = \mathbf{K}\boldsymbol{\epsilon}(\tilde{\mathbf{u}}^{res})$ the residual stress field. Of course, $\tilde{\boldsymbol{\sigma}}^{hand}_{PUM} = \tilde{\boldsymbol{\sigma}}^{hand}$ in Ω_1^{PUM}.

Once the set of n^{PUM} enriched vertices is defined, the new adjoint problem consists in finding $\tilde{\mathbf{u}}^{res} \in \boldsymbol{\mathcal{U}}_{ad,0}$ such that:

$$\begin{aligned}
\int_\Omega \tilde{\boldsymbol{\sigma}}^{res} : \boldsymbol{\epsilon}(\mathbf{v}) \mathrm{d}\Omega &= \int_\Omega \left(\tilde{\boldsymbol{\sigma}}_\Sigma : \boldsymbol{\epsilon}(\mathbf{v}) + \tilde{\mathbf{f}}_\Sigma \cdot \mathbf{v} \right) \mathrm{d}\Omega - \int_\Omega \tilde{\boldsymbol{\sigma}}^{hand}_{PUM} : \boldsymbol{\epsilon}(\mathbf{v}) \mathrm{d}\Omega \\
&= \int_{\Omega_1^{PUM}} \left(\tilde{\boldsymbol{\sigma}}_\Sigma : \boldsymbol{\epsilon}(\mathbf{v}) + \tilde{\mathbf{f}}_\Sigma \cdot \mathbf{v} - \tilde{\boldsymbol{\sigma}}^{hand} : \boldsymbol{\epsilon}(\mathbf{v}) \right) \mathrm{d}\Omega - \int_{\Omega_2^{PUM}} \tilde{\boldsymbol{\sigma}}^{hand}_{PUM} : \boldsymbol{\epsilon}(\mathbf{v}) \mathrm{d}\Omega \\
&= -\int_{\partial\Omega_1^{PUM}} \tilde{\boldsymbol{\sigma}}^{hand} \mathbf{n}_{12} \cdot \mathbf{v} \mathrm{d}S - \int_{\Omega_2^{PUM}} \tilde{\boldsymbol{\sigma}}^{hand}_{PUM} : \boldsymbol{\epsilon}(\mathbf{v}) \mathrm{d}\Omega \quad \forall \mathbf{v} \in \boldsymbol{\mathcal{U}}_{ad,0}
\end{aligned} \tag{37}$$

where $\mathbf{n}_{12}$ is the outgoing normal from Ω_1^{PUM} to Ω_2^{PUM}. The loading consists in tractions $-\tilde{\boldsymbol{\sigma}}^{hand}\mathbf{n}_{12}$ on $\partial\Omega_1^{PUM}$ and a pre-stress $-\tilde{\boldsymbol{\sigma}}^{hand}_{PUM}$ in Ω_2^{PUM}.

An accurate approximation $(\tilde{\mathbf{u}}^{res}_h, \tilde{\boldsymbol{\sigma}}^{res}_h)$ of the residual solution can be obtained with the initial mesh; the enrichment technique is thus non-intrusive in the sense that operators (stiffness matrix, mesh connectivities) defined for the primal problem can be reused without any change to solve the adjoint problem; only the loading has to be modified. The computation of an admissible stress field $\hat{\tilde{\boldsymbol{\sigma}}}$ is also performed in a non-intrusive way: one first defines a stress field $\hat{\tilde{\boldsymbol{\sigma}}}^{res}$ that satisfies (37), with the same method as that used to compute $\hat{\boldsymbol{\sigma}}$; we then define:

$$\hat{\tilde{\boldsymbol{\sigma}}} = \tilde{\boldsymbol{\sigma}}^{hand}_{PUM} + \hat{\tilde{\boldsymbol{\sigma}}}^{res} \tag{38}$$

Eventually, we obtain the following bounding:

$$|Q(\mathbf{u}) - Q(\mathbf{u}_h) - Q_{corr}| \leq \mathcal{E}_{CRE}(\mathbf{u}_h, \hat{\boldsymbol{\sigma}}).\mathcal{E}_{CRE}(\tilde{\mathbf{u}}_h^{res}, \hat{\tilde{\boldsymbol{\sigma}}}^{res}) \tag{39}$$

where the right-hand side is independent of the enrichment $(\tilde{\mathbf{u}}^{hand}, \tilde{\boldsymbol{\sigma}}^{hand})$. In practice, the CRE measure $\mathcal{E}_{CRE}(\tilde{\mathbf{u}}_h^{res}, \hat{\tilde{\boldsymbol{\sigma}}}^{res})$ on the residual adjoint solution is small, and (39) provides for very accurate bounds on the local error without remeshing.

The non-intrusive approach also permits one to consider a quantity of interest which is pointwise in space. In such as case, the loading of the adjoint problem is defined from Dirac functions, with possibly infinite energy solution. A classical method would consist in regularizing the quantity of interest, using for instance weighting functions (so-called mollifiers) [147], in order to preserve the regularity of the adjoint solution; the initial quantity of interest is then replaced with a weighted local average. With the non-intrusive approach, truly pointwise quantities can be addressed without resorting to any regularization, by using Green functions as local enrichment. In many cases, these functions can be determined analytically in a (semi-)infinite domain, e.g. see [122]; an example of such a function is given in Fig. 16. In more complex situations (anisotropic material for instance), Green functions may be obtained implicitly.

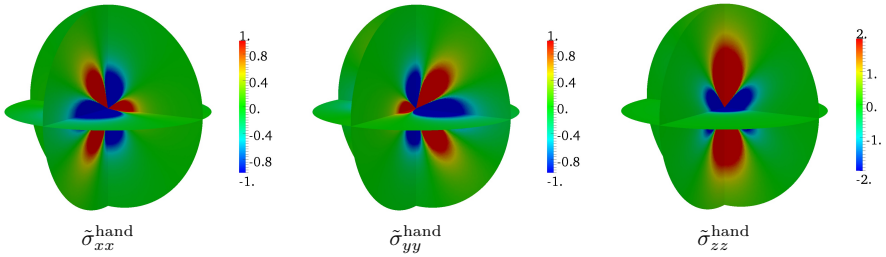

Figure 16: Stress field associated to a pointwise pre-stress in a 3D infinite domain.

Remark 9. *In addition to the non-intrusive approach, a technique was introduced in [110] in order to conserve guaranteed error bounds on nonlinear pointwise quantities of interest (such as the Von Mises equivalent stress). This technique is based on a decomposition of Q with projection properties in order to take higher-order terms into account in the bounds. It leads to the*

introduction of a set of extractors, and therefore to the parallel solution of a set of adjoint problems.

3.5. Extension to nonlinear problems

The goal-oriented approach using the CRE concept was extended to nonlinear materials behaviors in [107, 109]. In this context, and to preserve the property of guaranteed error bounds, a key point is the integration of the quantity of interest in terms of finite variations. This leads to the introduction of an auxiliary problem called the mirror problem, nonlinear and very similar to the primal problem, as a substitute to the classical (linear) adjoint problem. The mirror problem naturally coincides with the adjoint problem in the linear case.

Using notations of Section 2.5, the studied quantity of interest is written as:

$$Q = \int_0^T \int_\Omega \left[\boldsymbol{\sigma} : \delta\dot{\tilde{\boldsymbol{\Sigma}}} - \mathbf{Y} \cdot \delta\dot{\tilde{\mathbf{X}}} \right] \mathrm{d}\Omega \, \mathrm{d}t = \int_0^T \int_\Omega \mathbf{s} \cdot \delta\dot{\tilde{\mathbf{e}}}_\Sigma \mathrm{d}\Omega \, \mathrm{d}t \tag{40}$$

with the extraction function $\delta\dot{\tilde{\mathbf{e}}}_\Sigma \equiv \begin{bmatrix} \delta\dot{\tilde{\boldsymbol{\Sigma}}} \\ -\delta\dot{\tilde{\mathbf{X}}} \end{bmatrix}$ satisfying $\delta\dot{\tilde{\mathbf{e}}}_\Sigma = 0$ at $t = T$. Here, δ is a symbol indicating that $\delta\dot{\tilde{\mathbf{e}}}_\Sigma$ should be interpreted as a finite but relatively small variation, even though no linearization is carried out.

The mirror problem is then introduced, with a similar structure a for the primal problem except that time now goes backward. It is written with δ-quantities, over the space-time domain $\Omega \times [0, T]$ with time variable $\tau = T - t$, and it consists in finding the solution pair $(\delta\dot{\tilde{\mathbf{e}}}, \delta\tilde{\mathbf{s}})$ which satisfies the following conditions:

$$\begin{aligned}
&\bullet\ \delta\dot{\tilde{\mathbf{e}}} = \delta\dot{\tilde{\mathbf{e}}}_e + \delta\dot{\tilde{\mathbf{e}}}_p \text{ is kinematically admissible} \\
&\bullet\ \delta\tilde{\mathbf{s}} - \delta\tilde{\mathbf{s}}_\Sigma \text{ is statically admissible} \\
&\bullet\ \delta\tilde{\mathbf{e}}_e = \boldsymbol{\Lambda}(\delta\tilde{\mathbf{s}}) \quad \text{(state equations)} \\
&\bullet\ \delta\dot{\tilde{\mathbf{e}}}_p = \tilde{\mathbf{B}}(\delta\tilde{\mathbf{s}}) \equiv \mathbf{B}(\mathbf{s}_h + \delta\tilde{\mathbf{s}}) - \mathbf{B}(\mathbf{s}_h) \quad \text{(evolution laws)} \\
&\bullet\ \delta\tilde{\mathbf{s}} = \delta\dot{\tilde{\mathbf{e}}} = 0 \text{ at } \tau = 0 \quad \text{(initial conditions)}
\end{aligned} \tag{41}$$

$\mathbf{s}_h$ is the approximate FE solution of the primal problem, and $\delta\dot{\tilde{\mathbf{e}}}_\Sigma \equiv \tilde{\mathbf{B}}(\delta\tilde{\mathbf{s}}_\Sigma) + \boldsymbol{\Lambda}(\delta\dot{\tilde{\mathbf{s}}}_\Sigma)$.

Let $(\delta\dot{\tilde{\mathbf{e}}}_h, \delta\tilde{\mathbf{s}}_h)$ be the FE solution of the mirror problem, and $(\delta\dot{\hat{\tilde{\mathbf{e}}}}, \delta\hat{\tilde{\mathbf{s}}})$ an associated admissible solution over $\Omega \times [0,T]$. The following relation holds:

$$Q - Q_h - Q_{corr} = \int_0^T \int_\Omega \left(\mathbf{s} - \hat{\mathbf{s}}^m\right) \cdot \left(\delta\dot{\hat{\tilde{\mathbf{e}}}}_p - \tilde{\mathbf{B}}(\delta\hat{\tilde{\mathbf{s}}})\right) \mathrm{d}\Omega \, \mathrm{d}t - \mathbf{C}(\mathbf{s} - \mathbf{s}_h, \delta\tilde{\mathbf{s}}_\Sigma) + \mathbf{C}(\mathbf{s} - \mathbf{s}_h, \delta\hat{\tilde{\mathbf{s}}}) \tag{42}$$

with $\hat{\mathbf{s}}^m = \frac{1}{2}(\hat{\mathbf{s}} + \mathbf{s}_h)$ and:

$$\begin{aligned}
Q_{corr} = & - \int_0^T \int_\Omega \Big[\left(\dot{\mathbf{e}} - \dot{\mathbf{e}}_h\right) \cdot \left(\delta\tilde{\mathbf{s}}_\Sigma - \delta\hat{\tilde{\mathbf{s}}}\right) - \left(\hat{\mathbf{s}} - \mathbf{s}_h\right) \cdot \delta\dot{\hat{\tilde{\mathbf{e}}}} \\
& + \left(\hat{\mathbf{s}}^m - \mathbf{s}_h\right) \cdot \left(\tilde{\mathbf{B}}(\delta\hat{\tilde{\mathbf{s}}}) - \delta\dot{\hat{\tilde{\mathbf{e}}}}_p\right) \Big] \mathrm{d}\Omega \, \mathrm{d}t \\
\dot{\mathbf{e}}_h = & \boldsymbol{\Lambda}(\dot{\mathbf{s}}_h) + \mathbf{B}(\mathbf{s}_h) \\
\delta\dot{\hat{\tilde{\mathbf{e}}}}_{p|t} = & \left[\delta\tilde{\mathbf{e}}_{h,\tau} - \boldsymbol{\Lambda}(\delta\hat{\mathbf{s}}_\tau)\right]_{|\tau = T-t} \\
\mathbf{C}(\Delta\mathbf{s}, \delta\mathbf{s}) = & \int_0^T \int_\Omega [\Delta\mathbf{s} \cdot \delta\dot{\mathbf{e}}_p - \Delta\dot{\mathbf{e}}_p \cdot \delta\mathbf{s}] \mathrm{d}\Omega \, \mathrm{d}t \quad \text{with} \quad \Delta\dot{\mathbf{e}}_p = \tilde{\mathbf{B}}(\Delta\mathbf{s})
\end{aligned} \tag{43}$$

The $\mathbf{C}$-terms in (42) are very small provided the finite variations $(\mathbf{s} - \mathbf{s}_h)$ and $\delta\tilde{\mathbf{s}}_\Sigma$ are small; $\mathbf{C}$ is called the model nonlinearity indicator.

Upper error bounds can then be derived from (42); all details can be found in [107, 109]. Illustrations of such bounds can be found in [23] for viscoelasticity (taking history effects into account), in [158] for dynamics, or in [113] for viscoplasticity. Furthermore, the general case where the material operator $\mathbf{B}$ is not defined using two dual potentials (convex functions) but is simply maximum monotonous is given in [109].

4. Model updating with the CRE concept

In this section, we now couple the CRE concept with experimental data in order to address inverse problems and perform parameter identification.

4.1. Inverse analysis for parameter identification

We come back to the reference (here linear) elasticity problem given in Section 2.1, but we now place in a general and practical identification context at the structural scale. It corresponds to a ill-posed problem in which $\partial_1\Omega \cap \partial_2\Omega \neq \emptyset$ potentially, with additional experimental information available

in terms of observations $\mathbf{d}_{obs}$ given by sensors (see Fig. 17). These may be local or distributed kinematic quantities measured from strain gauges, cameras, optic fibers, etc. They are used to identify a set $\mathbf{p} \in \mathcal{P}$ of unknown (or only partially known) scalar constitutive parameters, such as elastic moduli, associated with material properties and feeding the overall model by means of the Hooke tensor $\mathbf{K}(\mathbf{p})$. The goal is to infer the missing knowledge on these parameters, usually chosen dimensionless, by exploiting the overabundant experimental information available. The procedure thus falls into the larger framework of inverse problems in which the best fit is searched by comparing model outputs $\mathbf{d}(\mathbf{u}(\mathbf{p}))$ and observed outputs $\mathbf{d}_{obs}$.

A major concern is the fact that the inversion process is plagued with several error and uncertainty sources, in particular:

- measurement noise (out of possible systematic measurement error) caused by the limited accuracy of sensing devices and signal processing. Considering an additive measurement noise $\boldsymbol{\epsilon}$, quantified or not, the observed outputs read $\mathbf{d}_{obs} = \mathbf{d}_{true} + \boldsymbol{\epsilon}$ with $\mathbf{d}_{true}$ the physical (undisturbed) observation value;

- model bias caused by an always approximate virtual representation of the physical reality. As a consequence, there is no value of $\mathbf{p}$ such that $\mathbf{d}(\mathbf{u}(\mathbf{p})) = \mathbf{d}_{true}$.

Measurement and model uncertainties combine in the difference $\mathbf{d}(\mathbf{u}(\mathbf{p})) - \mathbf{d}_{obs}$ between model prediction and experimental data. Therefore, a sound inversion procedure should account for these uncertainties. Also, we do not account for discretization error here, but it may additionally be taken into account (e.g., see [13]).

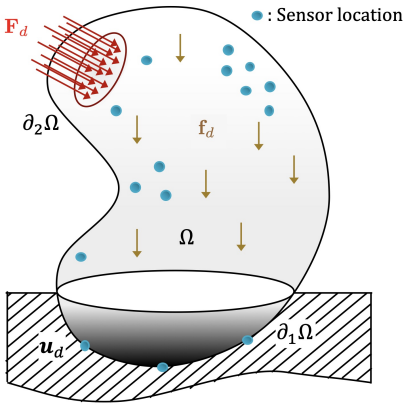

Figure 17: Configuration of the reference inverse problem.

In the following, we reuse admissibility spaces $\boldsymbol{\mathcal{U}}_{ad}$ and $\boldsymbol{\mathcal{S}}_{ad}$ defined in (4) and (5), respectively, and we introduce the additional space:

$$\boldsymbol{\mathcal{U}}^S_{ad,0} \equiv \left\{ \mathbf{v} \in [H^1(\Omega)]^d | \ \mathbf{v}_{|\partial\Omega\setminus\partial_2\Omega} = \mathbf{0} \right\} \supset \boldsymbol{\mathcal{U}}_{ad,0} \tag{44}$$

The weak form of equilibrium equations for the ill-posed inverse problem then reads:

$$-\int_\Omega \boldsymbol{\varpi} : \boldsymbol{\epsilon}(\mathbf{v}) \mathrm{d}\Omega + \int_\Omega \mathbf{f} \cdot \mathbf{v} \mathrm{d}\Omega + \int_{\partial_2\Omega} \mathbf{F} \cdot \mathbf{v} \mathrm{d}S = 0 \quad \forall \mathbf{v} \in \boldsymbol{\mathcal{U}}^S_{ad,0} \tag{45}$$

4.2. CRE-based model inversion

During the 1990s, the CRE functional was directly used to tackle the previously described inverse problem, as an alternative to conventional least square approaches used for parameter identification or updating. When unknown parameters are constitutive parameters, it is indeed a natural idea to consider a cost function that measures a residual on constitutive equations (which are less reliable than other equations of the problem) from an admissible solution. These equations are thus released with primal (displacement) and dual (stress) variables treated independently, so that the inverse problem is regularized by a lower constraint from the model. In this context of inverse analysis, the CRE functional is related to Kohn-Vogelius functionals introduced independently in conductivity imaging (electrical impedance tomography) [91]. It leads to a primal-dual formulation of inverse problems,

with physics-guided regularization (see [36] for a mathematical description on these aspects).

For the considered inverse problem, the CRE-based inverse strategy consists in choosing the CRE functional (11) as a cost function, and integrating the available experimental data as additional constraints to be fulfilled in a new definition of the admissibility space [96, 75, 68, 17]. Denoting by $(\mathbf{A}_d^+)$ this enriched admissibility space, in which observations are prescribed in addition to standard kinematic and static constraints, the resulting (constrained) optimization problem reads:

$$\mathbf{p}_{opt} = \underset{\mathbf{p}\in\mathcal{P}}{\arg\min} \left[\min_{(\hat{\mathbf{u}},\hat{\boldsymbol{\sigma}})\in(\mathbf{A}_d^+)} \mathcal{E}_{CRE}^2(\hat{\mathbf{u}},\hat{\boldsymbol{\sigma}};\mathbf{p}) \right] \quad ; \quad \mathcal{E}_{CRE}^2(\hat{\mathbf{u}},\hat{\boldsymbol{\sigma}};\mathbf{p}) = \frac{1}{2}\|\hat{\boldsymbol{\sigma}}-\mathbf{K}(\mathbf{p})\boldsymbol{\epsilon}(\hat{\mathbf{u}})\|_{\mathbf{K}^{-1}}^2 \tag{46}$$

This nonlinear problem is in practice solved iteratively, with sequential partial minimization over admissibility and parameters spaces. We note that the optimal admissible solution $(\hat{\mathbf{u}}_{opt},\hat{\boldsymbol{\sigma}}_{opt}) \in (\mathbf{A}_d^+)$ obtained at the end of the process satisfies a relation which is in general different from the constitutive relation of the model, except in the idealistic case where all admissibility conditions are compatible with the constitutive relation. This mismatch is directly measured by the CRE functional, with $\mathcal{E}_{CRE}(\hat{\mathbf{u}}_{opt},\hat{\boldsymbol{\sigma}}_{opt};\mathbf{p}_{opt}) > 0$.

The CRE strategy for inverse problems can be geometrically interpreted as shown in Fig. 18 (left). The minimal distance is searched between an admissible solution $(\hat{\mathbf{u}},\hat{\boldsymbol{\sigma}}) \in (\mathbf{A}_d^+)$ and the manifold $(\boldsymbol{\Gamma}_\mathbf{p})$ generated by the parametrized constitutive model. In most situations, $(\mathbf{A}_d^+) \cap (\boldsymbol{\Gamma}_\mathbf{p}) = \emptyset$.

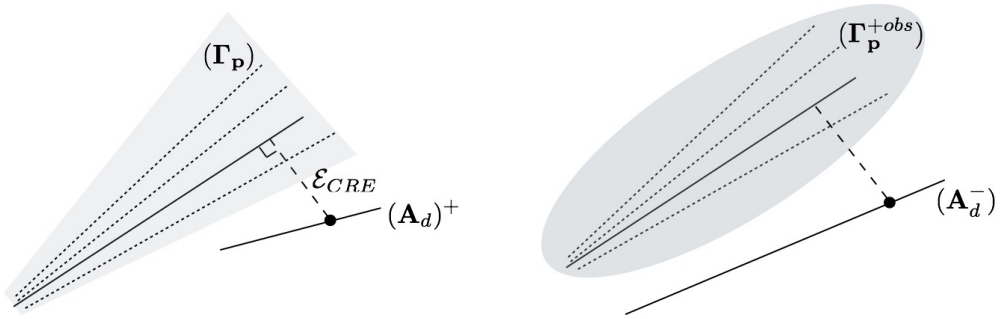

Figure 18: Geometrical interpretation of the CRE concept in inverse problems with $(\mathbf{A}_d^+) \cap (\mathbf{\Gamma_p}) = \emptyset$ (left), and of the mCRE with $(\mathbf{A}_d^-) \cap (\mathbf{\Gamma}_\mathbf{p}^{+obs}) = \emptyset$ (right).

4.3. Modified CRE

In the original CRE-based inversion procedure described above, strongly enforcing measured data as admissibility constraints is often inappropriate as these data are polluted with measurement noise, if not corrupted. A more flexible and effective approach consists in using a modified version of the CRE functional, called modified CRE (mCRE) and initially studied for model updating in vibration problems [96, 100]. This version conforms with a general philosophy in which a distinction is made between:

- reliable information on the inverse problem, such as equilibrium equations, location of sensors, or known boundary conditions;
- questionable information, such as the constitutive relation, noisy observation values, or imperfectly known boundary conditions (when applicable, e.g. see [65, 54]).

Only reliable information is enforced through a revisited definition of the admissibility space denoted $(\mathbf{A}_d^-)$, while remaining information is released and satisfied at best when minimizing an appropriate residual functional denoted $\mathcal{E}_{mCRE}$. The inverse procedure thus reads:

$$\mathbf{p}_{opt} = \underset{\mathbf{p}\in\mathcal{P}}{\arg\min} \left[\min_{(\hat{\mathbf{u}},\hat{\boldsymbol{\sigma}})\in(\mathbf{A}_d^-)} \mathcal{E}_{mCRE}^2(\hat{\mathbf{u}},\hat{\boldsymbol{\sigma}};\mathbf{p}) \right] \tag{47}$$

Considering for instance that only the constitutive relation and observation values are uncertain (i.e., $(\mathbf{A}_d^-) = \boldsymbol{\mathcal{U}}_{ad} \times \boldsymbol{\mathcal{S}}_{ad}$), the mCRE functional

reads:

$$\mathcal{E}^2_{mCRE}(\hat{\mathbf{u}}, \hat{\boldsymbol{\sigma}}; \mathbf{p}) = \mathcal{E}^2_{CRE}(\hat{\mathbf{u}}, \hat{\boldsymbol{\sigma}}; \mathbf{p}) + \frac{\alpha}{2}(\mathbf{d}(\hat{\mathbf{u}}) - \mathbf{d}_{obs})^T \mathbb{G}^{-1}_{obs}(\mathbf{d}(\hat{\mathbf{u}}) - \mathbf{d}_{obs}) \quad (48)$$

where $\mathbb{G}_{obs}$ is a scaling matrix and α is a positive scalar weight. Therefore, the mCRE cost function appears as a weighted combination between the CRE functional, which can be seen as a regularization term accounting for modeling error, and a classical least squares term of misfit between model predictions and observations. The optimal admissible solution $(\hat{\mathbf{u}}_{opt}, \hat{\boldsymbol{\sigma}}_{opt})$ obtained at the end of the inversion process results from a trade-off between modeling and experimental information, thus naturally defining a hybrid twin with data-based correction of the model ignorance as defined in [39].

A geometrical interpretation of the mCRE strategy is given in Fig. 18 (right); the minimal distance is searched between an admissible solution $(\hat{\mathbf{u}}, \hat{\boldsymbol{\sigma}}) \in (\mathbf{A}^-_d)$ and a manifold $(\boldsymbol{\Gamma}^{+obs}_{\mathbf{p}})$ generated by the parametrized constitutive model and noisy observations, with $(\mathbf{A}^-_d) \cap (\boldsymbol{\Gamma}^{+obs}_{\mathbf{p}}) = \emptyset$.

Remark 10. *The setting of the scalar weight α is a key aspect of the mCRE approach to avoid over-fitting or over-smoothing. Its influence on the quality of the mCRE-based inversion was illustrated in several works [51, 65, 8, 162]. Limit values of α correspond: (i) to the classical least-squares minimization with no modeling error taken into account a priori (emphasis put on satisfying the constitutive relation), when $\alpha \to 0$; (ii) to the pure CRE minimization with prescribed experimental data* (46)*, when $\alpha \to \infty$. The value of α should be conveniently set with regards to a priori quantitative information. This may be performed using the L-curve method [82], as implemented for mCRE in [86]. It may also be performed using the Morozov discrepancy principle [126, 127], as investigated in several recent works [129, 58], which relates the target distance between model predictions and observations to the measurement noise level.*

Remark 11. *A stochastic interpretation of the mCRE metric can be given [51], referring to the Bayesian inference framework and MAP estimator [155]. As an alternative to considering modeling error at measurement points by means of a covariance matrix (which is usually poorly known if not neglected), the mCRE strategy integrates modeling error in a global manner that allows for more flexibility in the model structure. It comes with a pdf*

$\pi_{mod} \propto e^{-\frac{\mathcal{E}^2_{CRE}(\hat{\mathbf{u}},\hat{\boldsymbol{\sigma}};\mathbf{p})}{\alpha}}$, *incorporated in the likelihood function, that quantitatively reflects the confidence on modeling.*

The minimization (47) of the mCRE functional is again performed by means of an iterative two-steps algorithm (alternating direction strategy of block Gauss-Seidel type), in which optimal admissible fields are first computed (for fixed $\mathbf{p}$), before minimizing the obtained cost function with respect to model parameters (for fixed admissible fields). Also, a convergence criterion is defined, such as a threshold ϵ on the value of the mCRE cost function (defined from a reference energy value). The algorithm thus reads:

0. Initialize the parameter set $\mathbf{p}^{(0)}$ and define the stopping criterion threshold ϵ
   Iteration loop (iteration $n+1$)
1. Compute optimal admissible fields $(\hat{\mathbf{u}}^{(n+1)}, \hat{\boldsymbol{\sigma}}^{(n+1)})$:

$$(\hat{\mathbf{u}}^{(n+1)}, \hat{\boldsymbol{\sigma}}^{(n+1)}) = \underset{(\hat{\mathbf{u}},\hat{\boldsymbol{\sigma}})\in(\mathbf{A}_d^-)}{\arg\min}\ \mathcal{E}^2_{mCRE}(\hat{\mathbf{u}}, \hat{\boldsymbol{\sigma}}; \mathbf{p}^{(n)}) \tag{49}$$

2. Update model parameters:

$$\mathbf{p}^{(n+1)} = \underset{\mathbf{p}\in\mathcal{P}}{\arg\min}\, \mathcal{F}_{mCRE}(\mathbf{p})\ ;\ \mathcal{F}_{mCRE}(\mathbf{p}) = \mathcal{E}^2_{mCRE}(\hat{\mathbf{u}}^{(n+1)}, \hat{\boldsymbol{\sigma}}^{(n+1)}; \mathbf{p}) \tag{50}$$

3. Stop if $\mathcal{F}_{mCRE}(\mathbf{p}^{(n+1)}) \leq \epsilon$, or increment n and go to Step 1

Alternatively, the stopping criterion may be based on the stagnation of the mCRE functional along successive iterations; this latter criterion may be more appropriate in some cases, particularly when the model has large bias.

Properties of the coupled system obtained at Step 1, resulting from the constrained minimization with search of the saddle point of a Lagrangian functional, were mathematically studied [7] and play a fundamental role in the qualitative and computational aspects of the mCRE minimization. It was shown that this specific system leads to a unique and stable solution (provided data is abundant enough) even in the case of missing information on boundary conditions for the forward problem. In addition, optimized numerical methods may be used to solve the coupled system. As an example, a (block) successive over-relaxation (SOR) technique was used in [8] in

the case of large-scale inverse identification, enabling for the use of existing parallel FE codes with minimal modifications. Also, the Sherman-Morrison-Woodbury formula was used in [120].
In Step 2 of the iterative algorithm, the nonlinear minimization may be advantageously conducted using a steepest descent approach. This takes advantage of good convexity properties of the mCRE functional, and of the fact that the gradient of this functional is easily computed using the adjoint-state method and available fields obtained at Step 1. In practice, a backtracking line search (Armijo-Goldstein rule) may be used to set the step length in the gradient algorithm, but other methods (e.g. BFGS or Gauss-Newton) may also be used.

Also, when $\mathbf{p}$ contains a large number of parameters (e.g. when describing a parameter field [8]), the spatial distribution of the cost function $\mathcal{F}_{mCRE}(\mathbf{p})$ may be used to select and update only parameters that contribute most to the mismatch [50], in addition to detecting corrupted sensors. This is the so-called localization step, performed at the end of Step 1. The associated hierarchical updating, with correction of parameters in zones with high local error alone (similarly to mesh adaptation procedures), is associated with a minimization problem in a lower-dimension parameter space. It thus reduces the computational cost and participates in the regularization process by guiding the identification/updating (since naturally favoring an optimal configuration close to the initial one). Zones may correspond to substructures in engineering applications, or to finite elements when identifying a parameter field, and additional techniques such as clustering can also be used [58].

Remark 12. *A goal-oriented variant of the mCRE approach was proposed in [26, 59], with automatic selection of the subset of parameters impacting a quantity of interest for identification purposes. This leads to a reduced computational cost while ensuring the accuracy of the prediction on the quantity of interest.*

Remark 13. *The iterative procedure used to minimize the mCRE functional is multi-query, as a series of similar systems (with different values for* $\mathbf{p}$*) needs to be solved to define the saddle-point of the Lagrangian and compute gradients of the cost function. Therefore, to highly reduce the computational cost, ROM techniques may be used [50, 21, 27].*

4.4. Numerical illustration

In the following numerical illustration, coming from a work reported in [129], we consider a numerical experiment with a biaxial test shown in Fig. 19. A cross-shaped specimen is biaxially loaded in a multiaxial testing machine. The studied material is made of a vinylister matrix reinforced by glass fibers. The quasi-uniform distribution of fiber orientations leads to an isotropic elastic behavior prior to heterogeneous matrix cracking and fiber breakage. We also consider experimental data in terms of full-field measurements obtained from quantitative imaging by means of Digital Image Correlation (DIC) techniques [154, 84]. The measurement zone is indicated with the red rectangle in Fig. 19; the experimental displacement field $\mathbf{u}_{obs}$ is measured by taking images with a CDD camera (resolution of 1008×1016 pixels) at the various loading steps. The reference picture for the DIC analysis is shown in Fig. 20; the DIC mesh is made of 781 nodes, also corresponding to the simulation mesh in the mCRE-based identification strategy.

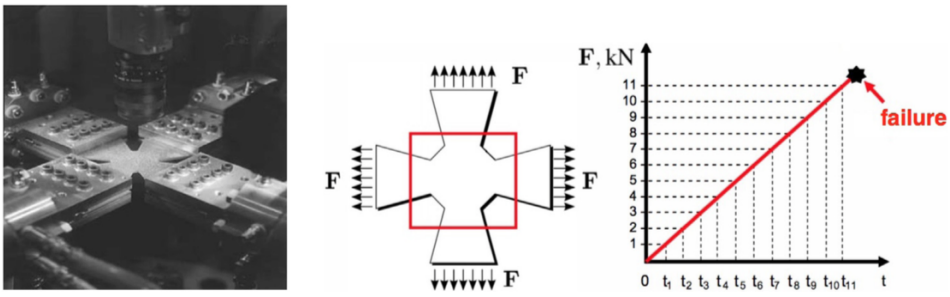

Figure 19: Biaxial test of a cross-shaped composite specimen: experimental setup, measurement zone, and loading evolution.

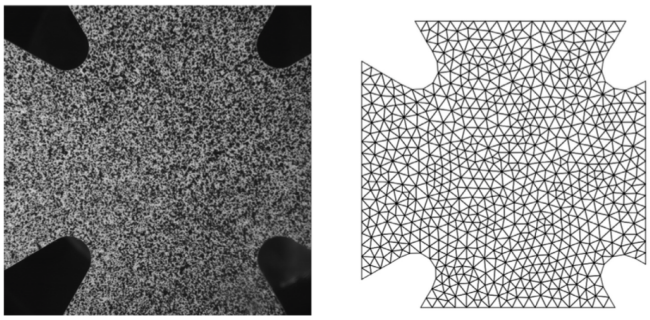

Figure 20: Reference picture for the DIC analysis and FEM discretization mesh for DIC.

Placing in the linear elasticity regime of the composite specimen (at time $t = t_5$ that is with a loading $F = 5$ kN), we wish to identify the Poisson ratio ν from mCRE and experimental information. The displacement field obtained from DIC is shown in Fig. 21. In order to implement the Morozov principle, we define the weighting factor as $\alpha = 10^{\beta}.\mathbf{U}_0^T\mathbb{K}_0\mathbf{U}_0$ where $\mathbf{U}_0$ and $\mathbb{K}_0$ are discretized displacement field and stiffness matrix associated with a reference solution. The obtained Morozov curve is shown in Fig. 22. When β is too small, there is a loss of information contained in the measurements and over-smoothing of the solution, resulting in values of the model-data discrepancy term larger than 1. Nevertheless, the curve does not go too high for small β, as admissible fields which are compared to measurements are already constructed from both model and measurements, so that model correction from experimental data is already performed. The curve indicates that the optimal weight value is here $\beta = 0$. For this value, the evolution of the mCRE cost function and its two components is displayed in Fig. 22; the attractive convexity property can be clearly observed. The identified value is $\nu_{opt}/\nu_0 = 1.24 \pm 0.14$. We represent in Fig. 23 the admissible fields $\hat{\mathbf{u}}$ and $\hat{\mathbf{v}}$ (associated with the admissible stress field), and their difference, obtained at the end of the identification process. Discrepancies between $\hat{\mathbf{u}}$ and $\hat{\mathbf{v}}$ are not so small as there is modeling error; large differences between both fields in the bottom left corner indicate that damage starts initiating there, as confirmed by experimental observations. We also show the comparison between the kinematically admissible field and the measured displacement field.

In order to show a practical interest of mCRE, we solve the identification

problem with reduced measurement zone. We analyze three configurations (see Fig. 24) in which we restrict experimental information in a subregion $\tilde{\Omega}_m$ corresponding to 64%, 36%, and 16% of the initial measurement zone Ω_m, respectively. In this process, admissibility conditions remain defined over the whole domain. The analysis with Morozov's principle (in order to set α) and the evolution of the mCRE functional are also shown in Fig. 24. Identification results are reported in Fig. 25, where we show the identified value ν_{opt} and its confidence interval for the various configurations. It appears that identification error increases with restricted experimental information, but it remains limited in all cases.

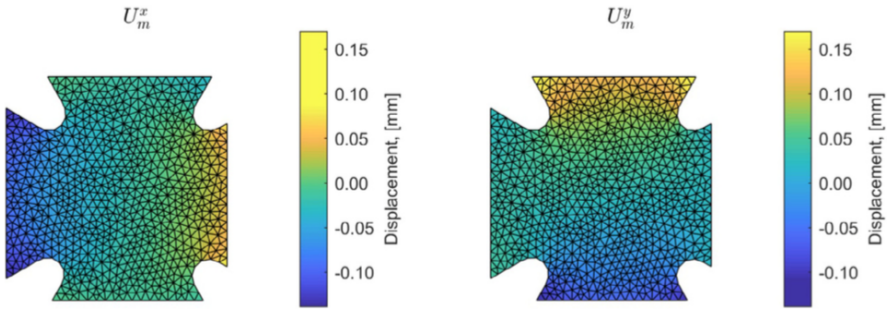

Figure 21: Horizontal and vertical components of the measured displacement field.

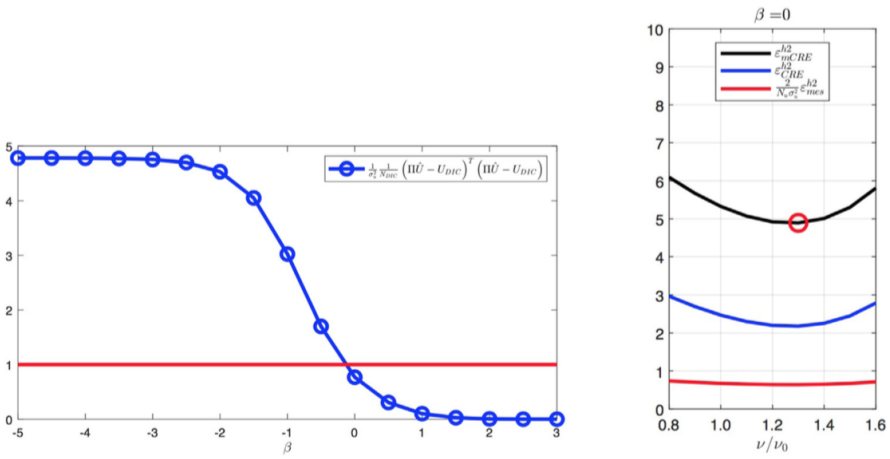

Figure 22: Evolution of the model-measurement mismatch term as a function of β, and evolutions of the mCRE functional and its two components as a function of ν for $\beta = 0$.

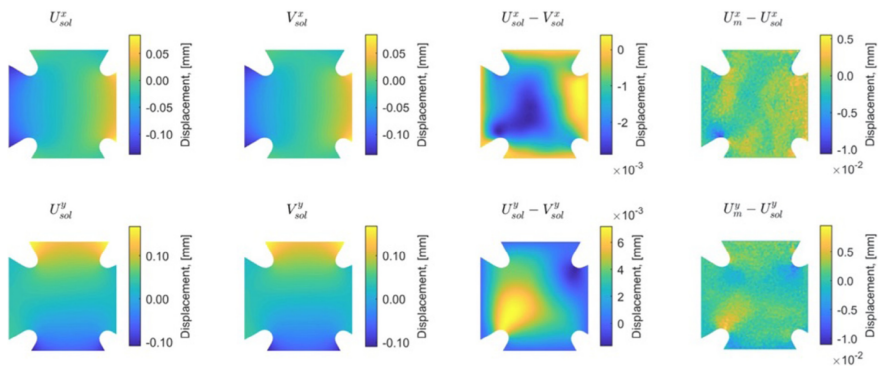

Figure 23: Spatial representation of admissible fields $\hat{\mathbf{u}}$, $\hat{\mathbf{v}}$, their difference, and $\mathbf{u}_{obs} - \hat{\mathbf{u}}$.

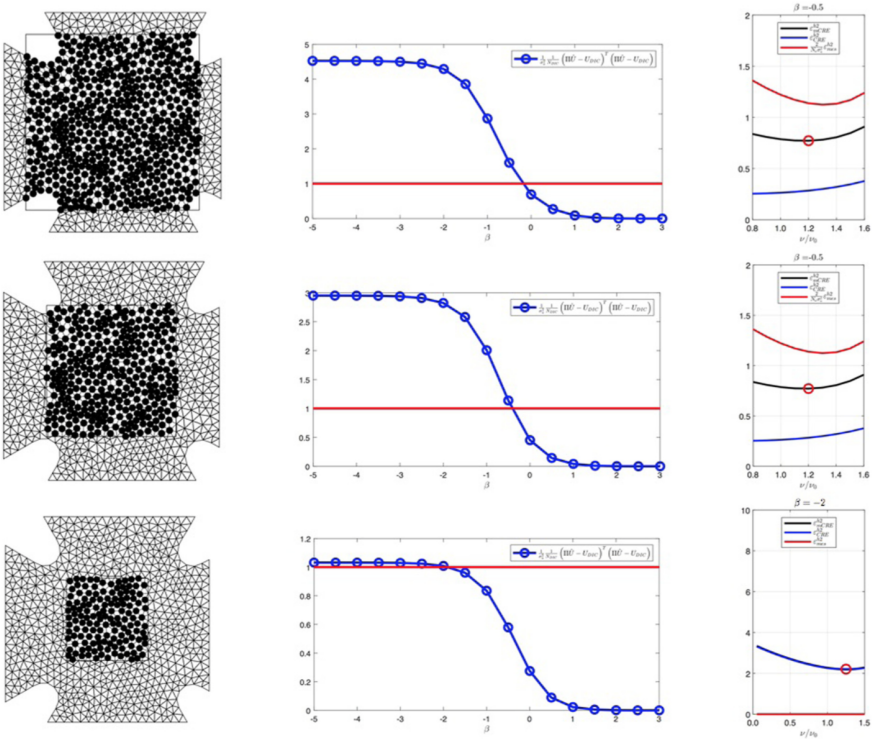

Figure 24: Various configurations with effective measurement zone $\tilde{\Omega}_m$, evolution of the measurement mismatch term as a function of β, and evolutions of the mCRE functional and its two components as a function of ν for optimal β.

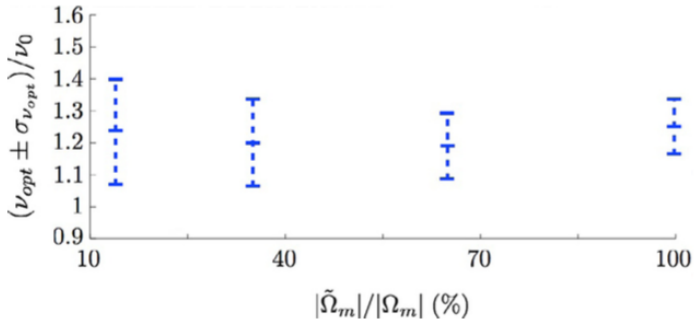

Figure 25: Identification results with restricted experimental information.

4.5. Towards sequential data assimilation

In the Dynamic Data Driven Applications Systems (DDDAS) framework, data is acquired sequentially and iteratively in time. A dedicated numerical process thus needs be used to infer noisy sequential measurement streams and recursively recover material state and model parameters. In this context, the mCRE was beneficially coupled in recent years with Kalman filtering and prediction/correction scheme (see Fig. 26) for sequential data assimilation [119, 56]. It leads to the Modified Dual Kalman Filter (MDKF) algorithm, benefiting from advantages of both mCRE and Kalman filtering approaches with increased robustness and capability for real-time data assimilation (e.g., using parallel computations); it permits to track evolving model parameters such as structural damage. In the MDKF strategy, the mCRE functional is actually used as a new metric in the observation space (compared to the classical L2-norm metric).

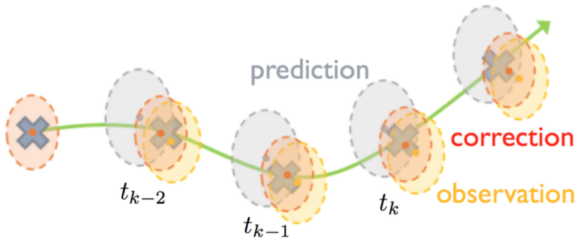

Figure 26: Sketch of the Kalman filtering recursive scheme with ovale shapes corresponding to confidence envelops of Gaussian distributions.

As an illustration, we detail a practical industrial application of MDKF reported in [56]. It deals with data assimilation on damageable structural systems in the context of earthquake engineering. The objective was to monitor in real-time, and from sparse acceleration measurements, the changing modal signature of a complex reinforced concrete specimen placed on a shaking table and undergoing nonlinear damage phenomena when submitted to low-frequency dynamic loadings (Fig. 27). The experimental database consisted in a sequence of gradually damaging tests, with some accelerometers placed on the structure, and the mCRE was written in the frequency domain. A typical result is given in Fig. 28, showing the predicted evolution of

the first eigenfrequency. One can clearly observe the frequency drops due to progressive structural damage during the dynamics test; these are effectively captured in real-time by means of the updated digital twin. This further enables an appropriate evolving online command on the shaking table, within a state feedback control strategy, taking into account the interaction between actuators, table, and the damaging specimen (all details can be found in [56]).

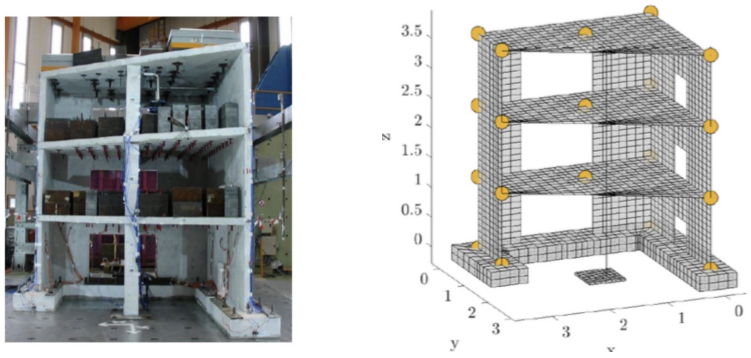

Figure 27: Concrete specimen anchored on the shaking table, and FE model with sensor locations.

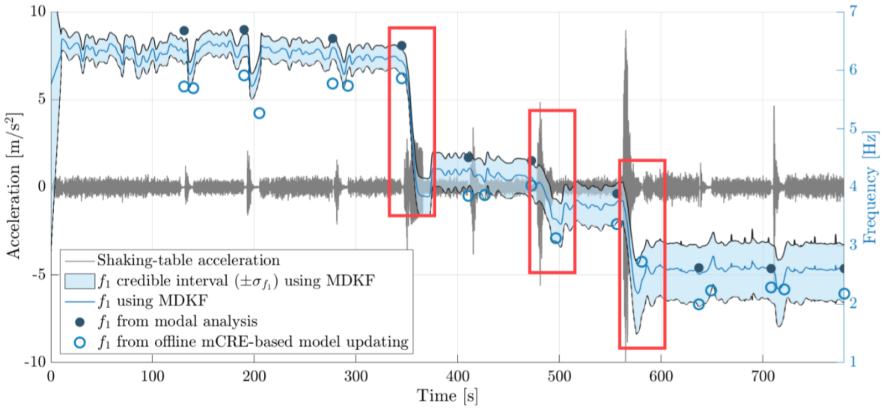

Figure 28: Predicted evolution of the first eigenfrequency using MDKF.

5. Model selection with the CRE concept

In this last section, we indicate some recent works which take advantage of the CRE measure, seen as a modeling error indicator defined over the whole domain, in order to improve the initial constitutive model. Whereas the structure of this model was supposed to fit within a given parametric representation in the previous section, here this structure is let free and is searched as optimal with respect to experimental observations. In other words, the constitutive model is adjusted so that it is consistent with data content and noise. A geometrical interpretation of the approach is given in Fig. 29.

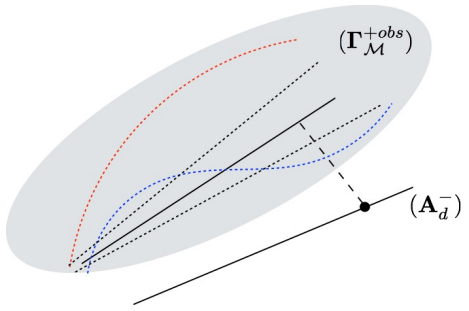

Figure 29: Geometrical interpretation of model selection from CRE information.

5.1. Model enrichment

A first possibility is to adaptively select the optimal constitutive model in a manifold $\mathcal{M}$ of model classes with increasing complexity levels (i.e., in a hierarchical list of model classes). Deviations between model predictions and observations are then adjusted so that model complexity and outputs remain consistent with data and measurement noise level. Using identification with mCRE, this model selection strategy was illustrated in [130] using the inverse problem with full-field measurements shown in Section 4.4, when the specimen is loaded in its nonlinear regime. The CRE term of the mCRE functional is then post-processed to drive the model complexity; a perfect match between model and measurements would correspond to a relative CRE value of the order of 1 when normalization and the Morozov principle are implemented. We show below the relative value of the CRE term for various model classes with increasing relevance with regards to the DIC measurements.

Table 1: Relative CRE value for various model classes

Model class	**Relative CRE value**
Isotropic elasticity	17.56
Orthotropic elasticity	3.27
Elasto-plasticity (Prandtl-Reuss)	2.29

5.2. Model learning

Another possibility to enhance the constitutive law representation is to learn model ignorance from data. This refers to data-driven modeling of complex materials from deep learning, which has become a very active research work [87, 121, 83] with pioneering contributions in [90, 88]. In this context, and relying on the mCRE framework, the NN-mCRE approach for unsupervised learning of state and evolution laws with a neural network (NN) was investigated in [15, 16]. This approach naturally focuses the strategy on what needs to be learnt, that is the constitutive relation, and it permits a data-based enrichment of an a priori constitutive model.
NN-mCRE aims at learning thermodynamic potentials (ψ, φ) introduced in Section 2. It integrates all the recent trends on learning (physics-informed, physics-augmented, transfer learning) by: (i) the specific definition of the loss function which exactly corresponds to the mCRE functional, with a priori physics constraints that are strongly enforced and clear convergence criteria; (ii) the chosen architecture of the NNs, employing input convex NNs (ICNNs) developed in [6] (see Fig. 30), to ensure thermodynamics consistency (additional classes of symmetry may also be added in the network architecture); (iii) the physics-guided initialization of the NNs, using a preliminary supervised training from an a priori constitutive model. Furthermore, it was shown that hyper-parameters of the NN-mCRE approach (learning rate, number of epochs, batch size, etc.) could be automatically and adaptively tuned, which is an important feature for online training as envisioned in DDDAS applications such as integrated SHM [32, 34]. The NN-mCRE approach performs by solving the minimization problem (47) where $\mathbf{p}$ now denotes weights and biases in ICNNs used to represent thermodynamic potentials.

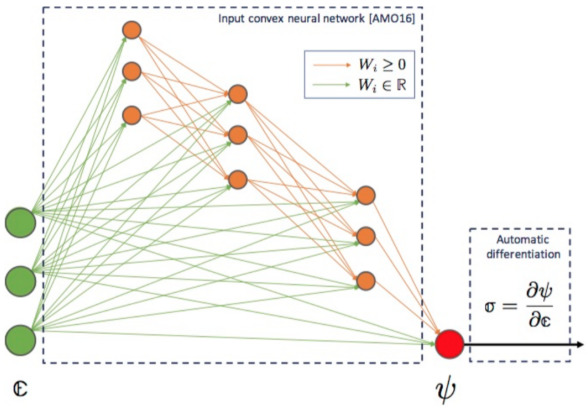

Figure 30: ICNN architecture used fo represent the thermodynamic potential.

We illustrate the NN-mCRE method using a reference non-quadratic potential ψ on state equations, that distinguishes behaviors in traction and compression along the longitudinal axis of a beam specimen; it reads in 2D and in the small strain regime:

$$\psi(\boldsymbol{\epsilon}) = \frac{1}{2}E_+\langle\epsilon_{11}\rangle_+^2 + \frac{1}{2}E_-\langle\epsilon_1 1\rangle_-^2 + \frac{1}{2}E\epsilon_{22}^2 + G\epsilon_{12}^2 \tag{51}$$

where $\langle\bullet\rangle_+$ (resp. $\langle\bullet\rangle_-$) denotes the positive (resp. negative) part. This potential is learnt from data, initializing the ICNN network with a linear elasticity model (quadratic potential). The database includes different loading cases with a combination of pure bending, traction and compression, and additional Gaussian measurement noise. Some results are given in Fig. 31, where we show how the constitutive model bias is correctly learnt during the NN-mCRE process (with high robustness to noise) and how the convergence rate of the training is insensitive to initial user-defined hyper-parameters

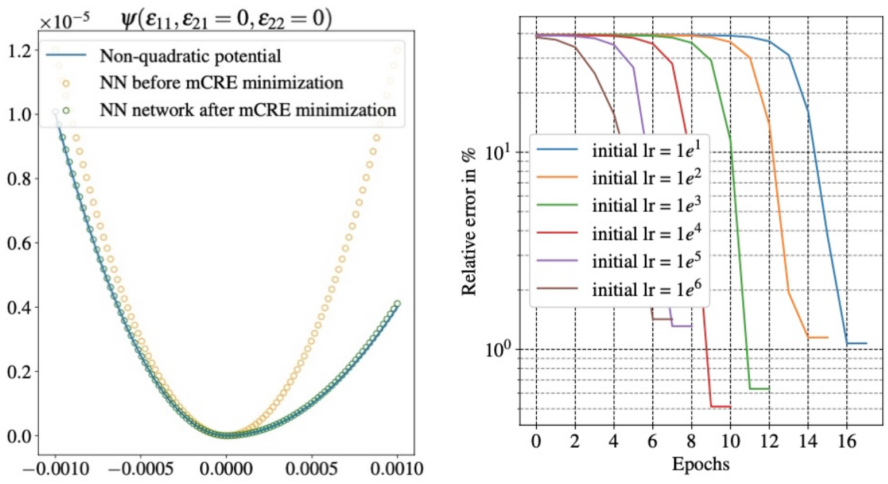

Figure 31: Initial and final potentials defined by the neural network, and convergence of the error for various initial learning rates.

Eventually, we also mention the recent work [116] in which data-driven material modeling from the CRE concept is discussed. A major aspect is that it answers the question of the mathematical model form of the most general data-driven model for stable materials (elasto-visco-plastic) taking physics and material science knowledge into account. It is shown that the data-driven model is the minimizer of the CRE functional, and can be obtained by implementing convex optimization with often explicit formulations.

Funding & Acknowledgements. L. Chamoin acknowledges the funding from the European Research Council (ERC) under the European Union's Horizon 2020 research and innovation program (grant agreement No. 101002857).

References

[1] Ainsworth M, Oden JT (1993) A unified approach to a posteriori error estimation using element residual methods. *Numerische Mathematik* **65**:23–50

[2] Ainsworth M, Oden JT (1997) A posteriori error estimation in finite element analysis. *Computer Methods in Applied Mechanics and Engineering* **142**(1-2):1–88

[3] Allier PE, Chamoin L, Ladevèze P (2015) Proper Generalized Decomposition computational methods on a benchmark problem: introducing a new strategy based on Constitutive Relation Error minimization. *Advanced Modeling and Simulation in Engineering Sciences* **2**:17

[4] Allier PE, Chamoin L, Ladevèze P (2018) Towards simplified and optimized a posteriori error estimation using PGD reduced models. *International Journal for Numerical Methods in Engineering* **113**(6):967–998

[5] Allix O, Feissel P, Nguyen HM (2005) Identification strategy in the presence of corrupted measurements. *Engineering Computations* **22**(5-6):487–504

[6] Amos B, Xu L, Kolter J (2017) Input convex neural networks. *Proceedings of the 34th International Conference on Machine Learning* **70**146–155

[7] Aquino W, Bonnet M (2019) Analysis of the error in constitutive equation approach for time-harmonic elasticity imaging. *SIAM Journal on Applied Mathematics* **79**:822–849

[8] Banerjee B, Walsh TF , Aquino W, Bonnet M (2013) Large scale parameter estimation problems in frequency-domain elastodynamics using an error in constitutive equation functional. *Computer Methods in Applied Mechanics and Engineering* **253**:60–72

[9] Banerjee RE, Weiser A (1985) Some a posteriori error estimators for elliptic partial differential equations. *Mathematics of Computation* **44**:283–301

[10] Barbarella E, Allix O, Daghia F, Lamon J, Jolivet T (2016) A new inverse approach for the localization and characterization of defects based on compressive experiments. *Computational Mechanics* **57**(6):1061–1074

[11] Barthe D, Deraemaeker A, Ladevèze P, Le Loch S (2004) Validation and updating of industrial models based on the constitutive relation error. *AIAA Journal* **42**(7):1427–1434

[12] Becker R, Rannacher R (1996) A feed-back approach to error control in finite element methods: Basic analysis and examples. *East-West Journal of Numerical Mathematics* **4**:237–264

[13] Becker R, Vexler B (2004) A posteriori error estimation for finite element discretization of parameter identification problems. *Numerische Mathematik* **96**(3):435–459

[14] Ben Azzouna M, Feissel P, Villon P (2015) Robust identification of elastic properties using the modified constitutive relation error. *Computer Methods in Applied Mechanics and Engineering* **295**:196–218

[15] Benady A, Baranger E, Chamoin L (2024) NN-mCRE: A modified Constitutive Relation Error framework for unsupervised learning of nonlinear state laws with physics-augmented Neural Networks. *International Journal for Numerical Methods in Engineering* **125**(8):e7439

[16] Benady A, Baranger E, Chamoin L (2024) Unsupervised learning of history-dependent constitutive material laws with thermodynamically-consistent neural networks in the modified Constitutive Relation Error framework. *Computer Methods in Applied Mechanics and Engineering* **425**:116967

[17] Blaysat B, Florentin E, Lubineau G, Moussawi A (2012) A dissipation gap method for full-field measurement-based identification of elastoplastic material parameters. *International Journal for Numerical Methods in Engineering* **91**(7):685–704

[18] Bonnet M, Constantinescu A (2005) Inverse problems in elasticity. *Inverse Problems* **21**:R1–R50

[19] Bonnet M, Aquino W (2015) Three-dimensional transient elastodynamic inversion using an error in constitutive relation functional,. *Inverse Problems* **31**:035010

[20] Boroomand B, Zienkiewicz OC (1997) Recovery by equilibrium in patches (REP). *International Journal for Numerical Methods in Engineering* **40**:137–164

[21] Bouclier R, Louf F, Chamoin L (2013) Real-time validation of mechanical models coupling PGD and constitutive relation error. *Computational Mechanics* **52**(4):861–883

[22] Bui H, Constantinescu A (2000) Spatial localization of the error of constitutive law for the identification of defects in elastic bodies. *Archives of Mechanics* **52**(4-5):511–522

[23] Chamoin L, Ladevèze P (2007) Bounds on history-dependent or independent local quantities in viscoelasticity problems solved by approximate methods. *International Journal for Numerical Methods in Engineering* **71**(12):1387–1411

[24] Chamoin L, Ladevèze P (2008) A non-intrusive method for the calculation of strict and efficient bounds of calculated outputs of interest in linear viscoelasticity problems. *Computer Methods in Applied Mechanics and Engineering* **197**(9-12):994–1014

[25] Chamoin L, Florentin E, Pavot S, Visseq V (2012) Robust goal-oriented error estimation based on the constitutive relation error for stochastic problems. *Computers and Structures* **106-107**:189–195

[26] Chamoin L, Ladevèze P, Waeytens J (2014) Goal-oriented updating of mechanical models using the adjoint framework. *Computational Mechanics* **54**(6):1415–1430

[27] Chamoin L, Allier PE, Marchand B (2016) Synergies between the Constitutive Relation Error concept and PGD model reduction for simplified V&V procedures. *Advanced Modeling and Simulation in Engineering Sciences* **3**:18

[28] Chamoin L, Pled F, Allier PE, Ladevèze P (2017) A posteriori error estimation and adaptive strategy for PGD model reduction applied to parametrized linear parabolic problems. *Computer Methods in Applied Mechanics and Engineering* **327**:118–146

[29] Chamoin L, Legoll F (2018) A posteriori error estimation and adaptive strategy for the control of MsFEM computations. *Computer Methods in Applied Mechanics and Engineering* **336**:1–38

[30] Chamoin L, Thai HP (2019) Certified real-time shape optimization using isogeometric analysis, PGD model reduction, and a posteriori error estimation. *International Journal for Numerical Methods in Engineering* **119**:151–176

[31] Chamoin L, Legoll F (2021) Goal-oriented error estimation and adaptivity in MsFEM computations. *Computational Mechanics* **67**(4):1201–1228

[32] Chamoin L (2021) DREAM-ON: merging advanced sensing techniques and simulation tools for future Structural Health Monitoring technologies. *The Project Repository Journal* **10**:124–127

[33] Chamoin L, Legoll F (2023) An introductory review on a posteriori error estimation in finite element computations. *SIAM Review* **65**(4):963–1028

[34] Chamoin L, Baranger E, Benady A, Charbonnel PE, Diaz M, Farahbakhsh S, Fribourg L, Martin-Xavier D, Poncelet M (2024) *A novel DDDAS architecture combining advanced sensing and simulation technologies for effective real-time structural health monitoring*. In "Handbook of Dynamic Data Driven Application Systems", vol. 3, Springer

[35] Charbonnel PE, Ladevèze P, Louf F, Le Noac'h C (2013) A robust CRE-based approach for model updating using in situ measurements. *Computers & Structures* **129**:63–73

[36] Chavent G, Kunisch K, Roberts J (1999) Primal-dual formulations for parameter estimation problems. *Journal of Computational and Applied Mathematics* **18**:173–229

[37] Chinesta F, Keunings R, Leygue A (2014) *The Proper Generalized Decomposition for Advanced Numerical Simulations*. Springer International Publishing

[38] Chinesta F, Huerta A, Rozza G, Wilcox K (2017) *Model reduction methods*. In "Encyclopedia of Computational Mechanics, 2nd Edition", vol. 1 Solids and Structures, Chapter 3, pp. 1–36, John Wiley & Sons

[39] Chinesta F, Cueto E, Abisset-Chavanne E, Duval JL, El Khaldi F (2020) Virtual, digital and hybrid twins: a new paradigm in data-based engineering and engineered data. *Archives of Computational Methods in Engineering* **27**:105–134

[40] Choi HW, Paraschivoiu M (2004) Adaptive computations of a posteriori finite element output bounds: a comparison of the "hybrid-flux" approach and the "flux-free" approach. *Computer Methods in Applied Mechanics and Engineering* **193**:4001–4033

[41] Chouaki A, Ladevèze P, Proslier L (1996) An updating of structural dynamic model with damping. *Inverse Problems in Engineering: Theory and Practice*:335–342

[42] Chouaki A, Ladevèze P, Proslier L (1998) Updating structural dynamic models with emphasis on the damping properties. *AIAA Journal* **36**(6):1094–1099

[43] Combe JP, Ladevèze P, Pelle JP (1999) Constitutive relation error estimator for transient finite element analysis. *Computer Methods in Applied Mechanics and Engineering* **176**:165–185

[44] Coorevits P, Hild P, Pelle JP (2000) A posteriori error estimation for unilateral contact with matching and non-matching meshes. *Computer Methods in Applied Mechanics and Engineering* **186**:65–83

[45] Cottereau R, Diez P, Huerta A (2009) Strict error bounds for linear solid mechanics problems using a subdomain based flux-free method. *Computational Mechanics* **44**(4):533–547

[46] Darema F (2015) DDDAS, A key driver for large-scale-big-data and large-scale-big-computing. *Procedia Computer Science* **51**:2463

[47] Debongnie JF, Zhong HG, Beckers P (1995) Dual analysis with general boundary conditions. *Computer Methods in Applied Mechanics and Engineering* **122**:183–192

[48] Decouvreur V, Bouillard P, Deraemaeker A, Ladevèze P (2004) Updating 2D acoustic models with the constitutive relation error method. *Journal of Sound and Vibration* **278**(4-5):773–787

[49] Decouvreur V, Deraemaeker A, Ladevèze P, Bouillard P (2007) Building a suited reduced modal basis for updating 3d acoustic models with the constitutive law error method. *Computer Methods in Applied Mechanics and Engineering* **196**(35-36):3400–3408

[50] Deraemaeker A, Ladevèze P, Leconte P (2002) Reduced bases for model updating in structural dynamics based on constitutive relation error. *Computer Methods in Applied Mechanics and Engineering* **191**(21):2427–2444

[51] Deraemaeker A, Ladevèze P, Romeuf T (2004) Model validation in the presence of uncertain experimental data. *Engineering Computations* **21**:808–833

[52] Destuynder P, Métivet B (1998) Explicit error bounds for a nonconforming finite element method. *SIAM Journal of Numerical Analysis* **35**(5):2099–2115

[53] Destuynder P, Métivet B (1999) Explicit error bounds in a conforming finite element method. *Mathematics of Computation* **68**(288):1379–1396

[54] Diaz MI, Aquino W, Bonnet M (2015) A modified error in constitutive equation approach for frequency-domain viscoelasticity imaging using interior data. *Computer Methods in Applied Mechanics and Engineering* **296**:129–149

[55] Diaz M, Charbonnel PE, Chamoin L (2022) Robust energy-based model updating framework for random processes in dynamics: application to shaking-table experiments. *Computers & Structures* **264**:106746

[56] Diaz M, Charbonnel PE, Chamoin L (2023) A new Kalman filter approach for structural parameter tracking: application to the monitoring of damaging structures tested on shaking tables. *Mechanical Systems and Signal Processing* **182**:109529

[57] Diaz M, Charbonnel PE, Chamoin L (2023) Merging experimental design and structural identification around the concept of modified Constitutive Relation Error in low-frequency dynamics for enhanced structural monitoring. *Mechanical Systems and Signal Processing* **197**:110371

[58] Diaz M, Charbonnel PE, Chamoin L (2023) Fully automated model updating framework for damage detection based on the modified Constitutive Relation Error. *Computational Mechanics* **73**:619–638

[59] Djatouti Z, Waeytens J, Chamoin L, Chatellier P (2021) Goal-oriented sensor placement and model updating strategies applied to a real building in the Sense-City equipment under controlled winter and heat wave scenarios. *Energy and Buildings* **231**:110486

[60] Ern A, Vohralik M (2010) A posteriori error estimation based on potential and flux reconstruction for the heat equation. *SIAM Journal on Numerical Analysis* **345**(48):198–223

[61] Ern A, Vohralik M (2015) Polynomial-degree-robust a posteriori estimates in a unified setting for conforming, nonconforming, discontinuous Galerkin, and mixed discretizations. *SIAM Journal on Numerical Analysis* **53**(2):1058–1081

[62] Farrar CR, Worden K (2007) An introduction to structural health monitoring. *Philosophical Transactions of the Royal Society A: Mathematical, Physical and Engineering Sciences* 365(1851):303–315

[63] Faverjon B, Sinou JJ (2008) Robust damage assessment of multiple cracks based on the frequency response function and the constitutive relation error updating method. *Journal of Sound and Vibration* **312**:821–837

[64] Faverjon B, Ladevèze P, Louf F (2009) Validation of stochastic linear structural dynamics models. *Computers & Structures* **87**(13-14):829–837

[65] Feissel P, Allix O (2007) Modified constitutive relation error identification strategy for transient dynamics with corrupted data: the elastic case. *Computer Methods in Applied Mechanics and Engineering* **196**:1968–1983

[66] Ferrier R, Cocchi A, Hochard C (2021) Modified constitutive relation error for field identification: theoretical and experimental assessments on fiber orientation identification in a composite material. *International Journal for Numerical Methods in Engineering* **122**(24):7553–7580

[67] Florentin E, Gallimard L, Pelle JP (2002) Evaluation of the local quality of stresses in 3D finite element analysis. *Computer Methods in Applied Mechanics and Engineering* **191**:4441–4457

[68] Florentin E, Lubineau G (2010) Identification of the parameters of an elastic material model using the constitutive equation gap method. *Computational Mechanics* **46**:521–531

[69] Fraeijs de Veubeke B (2001) Displacement and equilibrium models in the finite element method. *International Journal for Numerical Methods in Engineering* **52**:287–342

[70] Gallimard L, Ladevèze P, Pelle JP (1996) Error estimation and adaptivity in elastoplasticity. *International Journal for Numerical Methods in Engineering* **39**:189–217

[71] Gallimard L, Panetier J (2006) Error estimation of stress intensity factors for mixed-mode cracks. *International Journal for Numerical Methods in Engineering* **68**(3):299–316

[72] Gallimard L (2009) A constitutive relation error estimator based on traction-free recovery of the equilibrated stress. *International Journal for Numerical Methods in Engineering* **78**(4):460–482

[73] Gant F, Rouch P, Louf F, Champaney L (2011) Definition and updating of simplified models of joint stiffness. *International Journal of Solids and Structures* **48**:775–784

[74] Germain P, Nguyen QS, Suquet P (1983) Continuum thermodynamics. *Journal of Applied Mechanics* **50**:1010–1020

[75] Geymonat G, Hild F, Pagano S (2002) Identification of elastic parameters by displacement field measurement. *Comptes Rendus de l'Académie des Sciences, Mécanique* **330**(6):403–408

[76] Ghosh S, Zou Z, Babaniyi O, Aquino W, Diaz M, Bayat M, Fatemi M (2017) Modified error in constitutive equations (mece) approach for ultrasound elastography. *Journal of the Acoustical Society of America* **142**(4):2084

[77] Giles MB, Süli E (2002) Adjoint methods for PDEs: a posteriori error analysis and postprocessing by duality. *Acta Numerica* **11**:145–236

[78] Guchhait S, Banerjee B (2015) Constitutive error based material parameter estimation procedure for hyperelastic material. *Computer Methods in Applied Mechanics and Engineering* **297**:455–475

[79] Guchhait S, Banerjee B (2015) Constitutive error based parameter estimation technique for plate structures using free vibration signatures. *Journal of Sound and Vibration* **419**:302–317

[80] Guo M, Haghighat E (2022) Energy-based error bound of physics-informed neural network solutions in elasticity. *Journal of Engineering Mechanics* **148**(9):04022038

[81] Halphen B, Nguyen QS (1975) On the generalized standard materials (in French: Sur les matériaux standards généralisés). *Journal de Mécanique* **14**(1):39–63

[82] Hansen P (1998) *Rank-Deficient and Discrete Ill-Posed Problems*. SIAM Philadelphia

[83] Hernández Q, Badías A, González D, Chinesta F, Cueto E (2021) Structure-preserving neural networks. *Journal of Computational Physics* **426**:109950

[84] Hild F, Roux S (2012) *Digital image correlation*. In "Optical Methods for Solid Mechanics. A Full-Field Approach", pp. 183–228, Wiley

[85] Hu X, Prabhu S, Atamturktur S, Cogan S (2017) Mechanistically-informed damage detection using dynamic measurements: Extended constitutive relation error. *Mechanical Systems and Signal Processing* **85**:312–328

[86] Huang S, Feissel P, Villon P (2016) Modified constitutive relation error: an identification framework dealing with the reliability of information. *Computer Methods in Applied Mechanics and Engineering* **311**:1–17

[87] Huang DZ, Xu K, Farhat C, Darve E (2020) Learning constitutive relations from indirect observations using deep neural networks. *Journal of Computational Physics* **416**:109491

[88] Ibanez R, Borzacchiello D, Aguado JV, Abisset-Chavanne E, Cueto E, Ladevèze P, Chinesta F (2017) Data-driven non-linear elasticity: constitutive manifold construction and problem discretization. *Computational Mechanics* **60**(5):813–826

[89] Kempeneers M, Debongnie JF, Beckers P (2009) Pure equilibrium tetrahedral finite elements for global error estimation by dual analysis. *International Journal for Numerical Methods in Engineering* **81**(4):513–536

[90] Kirchdoerfer T, Ortiz M (2016) Data-driven computational mechanics. *Computer Methods in Applied Mechanics and Engineering* **304**:81–101

[91] Kohn RV, Lowe BD (1988) A variational method for parameter identification. *ESAIM: Mathematical Modelling and Numerical Analysis* **22**(1):119–158

[92] Ladevèze P (1975) *Comparaison de modèles de milieux continus*. Thèse d'état, Univ. P. et M. Curie, Paris

[93] Ladevèze P, Leguillon D (1983) Error estimate procedure in the finite element method and application. *SIAM Journal of Numerical Analysis* **20**(3):485–509

[94] Ladevèze P, Pelle JP (1989) Accuracy in finite element computation for eigenfrequencies. *International Journal for Numerical Methods in Engineering* **28**:1929–1949

[95] Ladevèze P, Gastine JL, Marin P, Pelle JP (1992) Accuracy and optimal meshes in finite element computation for nearly incompressible materials. *Computer Methods in Applied Mechanics and Engineering* **94**(3):303–314

[96] Ladevèze P, Nedjar D, Reynier M (1994) Updating of finite element models using vibration tests. *AIAA Journal* **32**(7):1485–1491

[97] Ladevèze P, Maunder EAW (1996) A general method for recovering equilibrating element tractions. *Computer Methods in Applied Mechanics and Engineering* **137**:111–151

[98] Ladevèze P, Rougeot P(1997) New advances on a posteriori error on constitutive relation in finite element analysis. *Computer Methods in Applied Mechanics and Engineering* **150**:239–249

[99] Ladevèze P, Moës N (1998) A new a posteriori error estimation for nonlinear time-dependent finite element analysis. *Computer Methods in Applied Mechanics and Engineering* **157**:45–68

[100] Ladevèze P, Chouaki A (1999) Application of a posteriori error estimation for structural model updating. *Inverse Problems* **15**(1):49–58

[101] Ladevèze P (1999) *Nonlinear Computational Structural Mechanics - New Approaches and Non-Incremental Methods of Calculation*. Springer

[102] Ladevèze P, Moës N, Douchin B (1999) Constitutive relation error estimations for (visco) plasticity finite element analysis with softening. *Computer Methods in Applied Mechanics and Engineering* **176**:247–264

[103] Ladevèze P (2000) Constitutive error estimators for time-dependent non-linear FE analysis. *Computer Methods in Applied Mechanics and Engineering* **188**(4):775–788

[104] Ladevèze P (2001) Constitutive relation error estimations for finite element analyses considering (visco)-plasticity and damage. *International Journal for Numerical Methods in Engineering* **52**(5-6):527–542

[105] Ladevèze P, Pelle JP (2005) *Mastering Calculations in Linear and Nonlinear Mechanics*. Springer NY

[106] Ladevèze P, Puel G, Deraemaeker A, Romeuf T (2006) Validation of structural dynamics models containing uncertainties. *Computer Methods in Applied Mechanics and Engineering* **195**(4-6):373–393

[107] Ladevèze P (2006) Upper error bounds on calculated outputs of interest for linear and nonlinear structural problems. *Comptes Rendus Académie des Sciences - Mécanique* **334**:399–407

[108] Ladevèze P, Florentin E (2006) Verification of stochastic models in uncertain environments using the constitutive relation error method. *Computer Methods in Applied Mechanics and Engineering* **196**:225–234

[109] Ladevèze P (2008) Strict upper error bounds for calculated outputs of interest in computational structural mechanics. *Computational Mechanics* **42**(2):271–286

[110] Ladevèze P, Chamoin L (2010) Calculation of strict error bounds for finite element approximations of nonlinear pointwise quantities of interest. *International Journal for Numerical Methods in Engineering* **84**:1638–1664

[111] Ladevèze P, Chamoin L, Florentin E (2010) A new non-intrusive technique for the construction of admissible stress fields in model verification. *Computer Methods in Applied Mechanics and Engineering* **199**(9):766–777

[112] Ladevèze P, Chamoin L (2011) On the verification of model reduction methods based on the Proper Generalized Decomposition. *Computer Methods in Applied Mechanics and Engineering* **200**:2032–2047

[113] Ladevèze P, Blaysat B, Florentin E (2012) Strict upper bounds of the error in calculated outputs of interest for plasticity problems. *Computer Methods in Applied Mechanics and Engineering* **245-246**:194–205

[114] Ladevèze P, Pled F, Chamoin L (2013) New bounding techniques for goal-oriented error estimation applied to linear problems. *International Journal for Numerical Methods in Engineering* **93**:1345–1380

[115] Ladevèze P, Chamoin L (2016) *The Constitutive Relation Error Method: a general verification tool.* In "Verifying calculations, forty years on: an overview of classical verification techniques for FEM simulations", L. Chamoin & P. Diez (Eds.), SpringerBriefs

[116] Ladevèze P, Chamoin L (2024) Data-driven material modeling based on the Constitutive Relation Error. *Advanced Modeling and Simulation in Engineering Sciences*, submitted

[117] Louf F, Combe JP, Pelle JP (2003) Constitutive error estimator for the control of contact problems involving friction. *Computers and Structures* **81**(18-19):1759–1772

[118] Luce R, Wohlmuth BI (2005) A local a posteriori error estimator based on equilibrated fluxes. *SIAM Journal on Numerical Analysis* **42**(4):1394–1414

[119] Marchand B, Chamoin L, Rey C (2016) Real-time updating of structural mechanics models using Kalman filtering, modified Constitutive

Relation Error and Proper Generalized Decomposition. *International Journal for Numerical Methods in Engineering* **107**(9):786–810

[120] Marchand B, Chamoin L, Rey C (2019) Parameter identification and model updating in the context of nonlinear mechanical behaviors using a unified formulation of the modified constitutive relation error concept. *Computer Methods in Applied Mechanics and Engineering* **345**:1094–1113

[121] Masi F, Stefanou I (2022) Multiscale modeling of inelastic materials with thermodynamics-based artificial neural networks (tann). *Computer Methods in Applied Mechanics and Engineering* **398**:115190

[122] Mindlin RD (1936) Force at a point in the interior of a semi-infinite solid.. *Journal of Physics* **7**:195–202

[123] Moitinho de Almeida JP, Maunder EAW (2009) Recovery of equilibrium on star patches using a partition of unity technique. *International Journal for Numerical Methods in Engineering* **79**:1493–1516

[124] Moitinho de Almeida JP, Maunder EAW (2017) *Equilibrium finite element formulations*. Wiley

[125] Moreau JJ (1966) *Convexity and duality, Functional Analysis and Optimization*. Academic Press

[126] Morozov V (1968) The error principle in the solution of operational equations by the regularization method. *USSR Computational Mathematics and Mathematical Physics* **8**(2):63–87

[127] Nair MT, Schock E, Tautenhahn U (2003) Morozov's discrepancy principle under general source conditions. *Journal for Analysis and its Applications* **22**(1):199–214

[128] Nguyen H, Allix O, Feissel P (2008) A robust identification strategy for rate-dependent models in dynamics. *Inverse Problems* **24**:065006

[129] Nguyen H, Chamoin L, Ha Minh C (2022) mCRE-based parameter identification from full-field measurements: consistent framework, integrated version, and extension to nonlinear material behaviors. *Computer Methods in Applied Mechanics and Engineering* **400**:115461

[130] Nguyen HN, Chamoin L (2024) Model and mesh selection from a mCRE functional in the context of parameter identification with full-field measurements. *Computational Mechanics*, submitted

[131] Oberkampf W, Roy C (2010) *Verification and Validation in Scientific Computing*. Cambridge University Press

[132] Oliveira HL, Louf F, Gatuingt F (2016) MCRE applied to the structural joint parameter identification under vibrating regime. *Computers and Concrete* 11(1):1–25

[133] Oliveira H, Louf F, Hervé-Secourgeon E, Gatuingt F (2020) Wall-slab joint parameter identification of a reinforced concrete structure using possibly corrupted modal data. *International Journal for Numerical and Analytical Methods in Geomechanics* 44(1):19-39

[134] Pagano S, Bonnet M (2013) *Constitutive equation gap.* in "Full-Field Measurements and Identification in Solid Mechanics", Vol. 10, pp. 275–300, John Wiley & Sons

[135] Panetier J, Ladevèze P, Louf F (2009) Strict bounds for computed stress intensity factors. *Computers & Structures* **871**(15-16):1015–1021

[136] Panetier J, Ladevèze P, Chamoin L (2010) Strict and effective bounds in goal-oriented error estimation applied to fracture mechanics problems solved with the XFEM. *International Journal for Numerical Methods in Engineering* **81**(6):671–700

[137] Paraschivoiu M, Peraire J, Patera AT (1997) A posteriori finite element bounds for linear functional outputs of elliptic partial differential equations. *Computer Methods in Applied Mechanics and Engineering* **150**:289–312

[138] Pares N, Dıez P, Huerta A (2006) Subdomain-based flux-free a posteriori error estimators. *Computer Methods in Applied Mechanics and Engineering* **195**:297–323

[139] Pares N, Santos H, Diez P (2009) Guaranteed energy error bounds for the Poisson equation using a flux-free approach: solving the local problems in subdomains. *International Journal for Numerical Methods in Engineering* **79**:1203–1244

[140] Parret-Fréaud A, Rey C, Gosselet P, Feyel F (2010) Fast estimation of discretization error for FE problems solved by domain decomposition. *Computer Methods in Applied Mechanics and Engineering* **199**(49-52):3315–3323

[141] Pelle JP, Ryckelynck D (2000) An efficient adaptive strategy to master the global quality of viscoplastic analysis. *Computers & Structures* **78**(1-3):169–184

[142] Peraire J, Patera AT (1998) Bounds for linear-functional outputs of coercive partial differential equations: local indicators and adaptive refinements. In "Advances in Adaptive Computational Methods in Mechanics", LP. Ladevèze & JT. Oden (Eds.), Elsevier, pp. 199–216

[143] Pled F, Chamoin L, Ladevèze P (2011) On the techniques for constructing admissible stress fields in model verification: performances on engineering examples. *International Journal for Numerical Methods in Engineering* **88**(5):409–441

[144] Pled F, Chamoin L, Ladevèze P (2012) An enhanced method with local energy minimization for the robust a posteriori construction of equilibrated stress fields in finite element analyses. *Computational Mechanics* **49**(3):357–378

[145] Prager W, Synge JL (1947) Approximation in elasticity based on the concept of functions spaces. *Quarterly of Applied Mathematics* **5**:261–269

[146] Progneaux A, Bouillard P, Deraemaeker A (2015) A model updating technique based on the constitutive relation error for in situ identification of admittance coefficient of sound absorbing materials. *Journal of Vibration and Acoustics* 137(5):051013

[147] Prudhomme S, Oden JT (1999) On goal-oriented error estimation for elliptic problems: application to the control of pointwise errors. *Computer Methods in Applied Mechanics and Engineering* **176**:313–331

[148] Reis J, Moitinho de Almeida JP, Diez P, Zlotnik S (2020) Error estimation for PGD solutions: a dual approach. *International Journal for Numerical Methods in Engineering* **23**:5275–5294

[149] Rey V, Rey C, Gosselet P (2014) A strict error bound with separated contributions of the discretization and of the iterative solver in non-overlapping domain decomposition methods. *Computer Methods in Applied Mechanics and Engineering* **270**:293–303

[150] Rodenas JJ, Tur M, Fuenmayor FJ, Vercher A (2007) Improvement of the superconvergent patch recovery technique by the use of constraint equations: the SPR-C technique. *International Journal for Numerical Methods in Engineering* **70**(6):705–727

[151] Roussel A, Capaldo M, Chamoin L, Argaud JP (2022) Modified constitutive relation error for multi-physics wind turbine calibration. *Journal of Physics: Conference Series* **2265**:042040

[152] Samir Z, Chamoin L, Abbas M (2023) A domain decomposition strategy for mCRE-based model updating in dynamics. *Computer Methods in Applied Mechanics and Engineering* **416**:116348

[153] Silva T, Maia N (2017) Detection and localisation of structural damage based on the error in the constitutive relations in dynamics. *Applied Mathematical Modelling* **46**:736–749

[154] Sutton M, Orteu JJ, Schreier H (2009) *Image Correlation for Shape, Motion and Deformation Measurements : Basic Concepts, Theory and Applications*. Springer

[155] Tarantola A (2005) *Inverse problem theory and methods for model parameter estimation*. SIAM

[156] Thai HP, Chamoin L, Ha Minh C (2019) A posteriori error estimation for isogeometric analysis using the concept of Constitutive Relation Error. *Computer Methods in Applied Mechanics and Engineering* **355**:1062–1096

[157] Vohralik M (2008) A posteriori error estimation in the conforming finite element method based on its local conservativity and using local minimization. *Comptes Rendus Mathématique* **346**(11-12):687–690

[158] Waeytens J, Chamoin L, Ladevèze P (2012) Guaranteed error bounds on pointwise quantities of interest for transient viscodynamics problems. *Computational Mechanics* **49**(3):291–307

[159] Wang L, Zhong H (2015) Stable linear traction-based equilibrium elements for elastostatics: Direct access to linear statically admissible stresses and quadratic kinematically admissible displacements for dual analysis. *International Journal for Numerical Methods in Engineering* **101**(12):887–932

[160] Wang L, Zhong H (2015) A unified approach to strict upper and lower bounds of quantities in linear elasticity based on constitutive relation error estimation. *Computer Methods in Applied Mechanics and Engineering* **286**:332–353

[161] Wang L, Chamoin L, Ladevèze P, Zhong H (2016) Computable upper and lower bounds on eigenfrequencies. *Computer Methods in Applied Mechanics and Engineering* **302**:27–43

[162] Warner JE, Diaz MI, Aquino W, Bonnet M (2014) Inverse material identification in coupled acoustic-structure interaction using a modified error in constitutive equation functional. *Computational Mechanics* **54**:1–15

[163] Wiberg NE, Abdulwahab F, Ziukas S (1994) Enhanced superconvergent patch recovery incorporating equilibrium and boundary conditions. *International Journal for Numerical Methods in Engineering* **37**:3417–3440

[164] Zheng Q, Liu J, Wang L (2023) An equilibrium finite element method for contact problem with application to strict error estimation. *Computational Mechanics* **71**(1):55–70